ARL 64-19

AERODYNAMICS OF THE FREE AND FORCED OSCILLATION OF A DISK AT SUBSONIC SPEEDS

W. W. WILLMARTH
N. E. HAWK

THE UNIVERSITY OF MICHIGAN
ANN ARBOR, MICHIGAN

JANUARY 1964

Contract AF 33(616)-7628
Project 7064
Task 7064-02

AEROSPACE RESEARCH LABORATORIES
OFFICE OF AEROSPACE RESEARCH
UNITED STATES AIR FORCE
WRIGHT-PATTERSON AIR FORCE BASE, OHIO

FOREWORD

This interim technical report was prepared by The University of Michigan, Ann Arbor, Michigan, on Contract No. AF 33(616)-7628 for the Aerospace Research Laboratories, Office of Aerospace Research, United States Air Force. The research reported herein was accomplished on Task 7064-02, "Research on the Aerodynamics of Blunt Bodies" of Project 7064, "Aerothermodynamic Investigations in High Speed Flow" under the technical cognizance of Mr. Otto Walchner of the Hypersonic Research Laboratory, ARL.

The authors gratefully acknowledge the advice and assistance of Professor A. M. Kuethe of the Department of Aeronautical and Astronautical Engineering. Sincere gratitude is also expressed to Mr. Takao Ishii of the National Aerospace Laboratory, Tokyo, Japan, for first recognizing some of the statistical aspects of the problem. Professors R. M. Howe, E. E. Gilbert and E. O. Gilbert of the Department of Aeronautical and Astronautical Engineering provided many valuable suggestions regarding the use of the analog computer. Messrs. B. J. Tu, R. P. Marcel, R. L. Harvey, F. L. Donovan and R. J. Brando were most helpful in the construction of the equipment and execution of the experiments.

ABSTRACT

Detailed studies were made of the free and forced oscillation of disks constrained to rotate about a fixed axis normal to the free-stream velocity. When the disk is free to rotate it oscillates about its axis at a definite frequency but with slowly varying amplitude and phase. Analog computer elements were used to make detailed measurements of the static restoring moment, dynamic restoring moment, average damping moment, statistical properties of the disk motion, and the power spectrum of the fluctuating turbulent moment acting on a fixed disk.

The measurements show that the impressed forcing function that causes the oscillation originates in the turbulent fluctuations in the disk wake. Using the measurements and the theory for forced random oscillations of a linear system, good qualitative prediction was made of the oscillation frequency, in all cases, and the mean square oscillation amplitude, for one particular case with very low friction of the supporting pivot.

TABLE OF CONTENTS

LIST OF FIGURES

LIST OF FIGURES (Concluded)

NOMENCLATURE

C_m = M/qSd, aerodynamic moment coefficient.

C'_m = M'/qSd, turbulent exciting moment coefficient.

$C_{\dot{W}}$ = $M\dot{\theta}/qUS$, work rate coefficient.

C_{m_θ} = $\dfrac{\partial M/\partial\theta}{qSd}$, aerodynamic restoring moment coefficient.

$C_{m_{\dot{\theta}}}$ = $\dfrac{\partial M/\partial\left(\frac{\dot{\theta}d}{U}\right)}{qSd}$, aerodynamic damping coefficient.

d = disk diameter.

h = disk thickness.

I = disk moment of inertia, slug-ft^2.

I^* = $I/\rho d^5$, reduced inertia.

I^*_1 = $(8/\pi)I^*$.

M = aerodynamic moment acting on disk.

M' = turbulent exciting moment.

n = frequency of oscillation, cps.

N = $\omega t/2\pi$, number of cycles elapsed since $t = 0$.

q = $\rho U^2/2$, dynamic pressure.

r = radial distance from center of disk.

R = $d/2$.

Re = Reynolds number, $\rho Ud/\mu$.

S = disk area, $\pi d^2/4$.

t = time, sec.

U = stream speed, fps.

$\overline{\dot{W}}$ = average work rate on disk due to aerodynamic moment.

θ_o = disk angular amplitude, radians (unless otherwise specified).

ϕ = disk phase lead, radians (unless otherwise specified).

θ = $\theta_o(t) \cos(\omega t+\phi)$, radians (unless otherwise specified). $\theta = 0$ when disk is normal to flow. A positive rotation is defined to be counterclockwise as viewed from the top of the tunnel.

ρ = density of the air, slugs/ft^3.

ω = circular frequency of oscillation, rad/sec.

ω^* = $\omega d/U$, reduced frequency.

I. INTRODUCTION

The flight path and motion of bodies on which flow separation has a large effect on the pressure distribution cannot be determined from the equations of motion for the body and fluid. In most cases the only way to obtain information about the motion of such bodies is to simulate the flow over the body and measure the aerodynamic forces and moments produced by the separated unsteady flow field. The equations of motion for the body alone and the experimentally determined forces and moments are then used to determine the body motion. The results of this procedure are only as good as the degree of simulation between the experiments and the real motion and flow field.

We have chosen the disk as an extreme example of such a flow field and have designed a number of experiments to reveal some of the simplest features of the disk motions and of the forces and moments that act on the disk. We have already studied the case of freely falling disks and discovered that above a certain critical Reynolds number, between 100 and 170 depending on the moment of inertia of the disk, unsteady fall was observed. At higher Reynolds numbers the unsteady motions most often observed were translational oscillations of the disk coupled with pitching oscillations about a diameter. A detailed description of the phenomena can be found in Ref. 1.

In order to determine the aerodynamic phenomena associated with the unsteady oscillating motion of the disks, we have made detailed studies of the free and forced oscillation of disks constrained to rotate about a fixed axis. In the case of free oscillations we observed that the disk oscillates about its diameter at a definite frequency but with varying amplitude and phase. Figure 1 shows records of disk orientation as a function of time. It appears from these records that the amplitude and phase vary slowly enough to allow one to define a definite frequency of oscillation almost all the time. The record of the disk motion resembles the response of a lightly damped harmonic oscillator to a random forcing function (a harmonic wave analyzer).

We designed a number of experiments to determine the nature of the driving force for the motion and the nature of the motion itself. The rather detailed experiments have two purposes: first, to reveal by studying a simple example, the important features of this and similar problems, and second, to develop methods and techniques for use in problems of this nature.

We shall first outline the theory for the disk motion and then describe the experimental equipment. The measurements of the observed disk motion during free oscillation are then described. The succeeding sections deal with measurements of the

Manuscript released November, 1963, by the authors for publication as an ARL Technical Documentary Report.

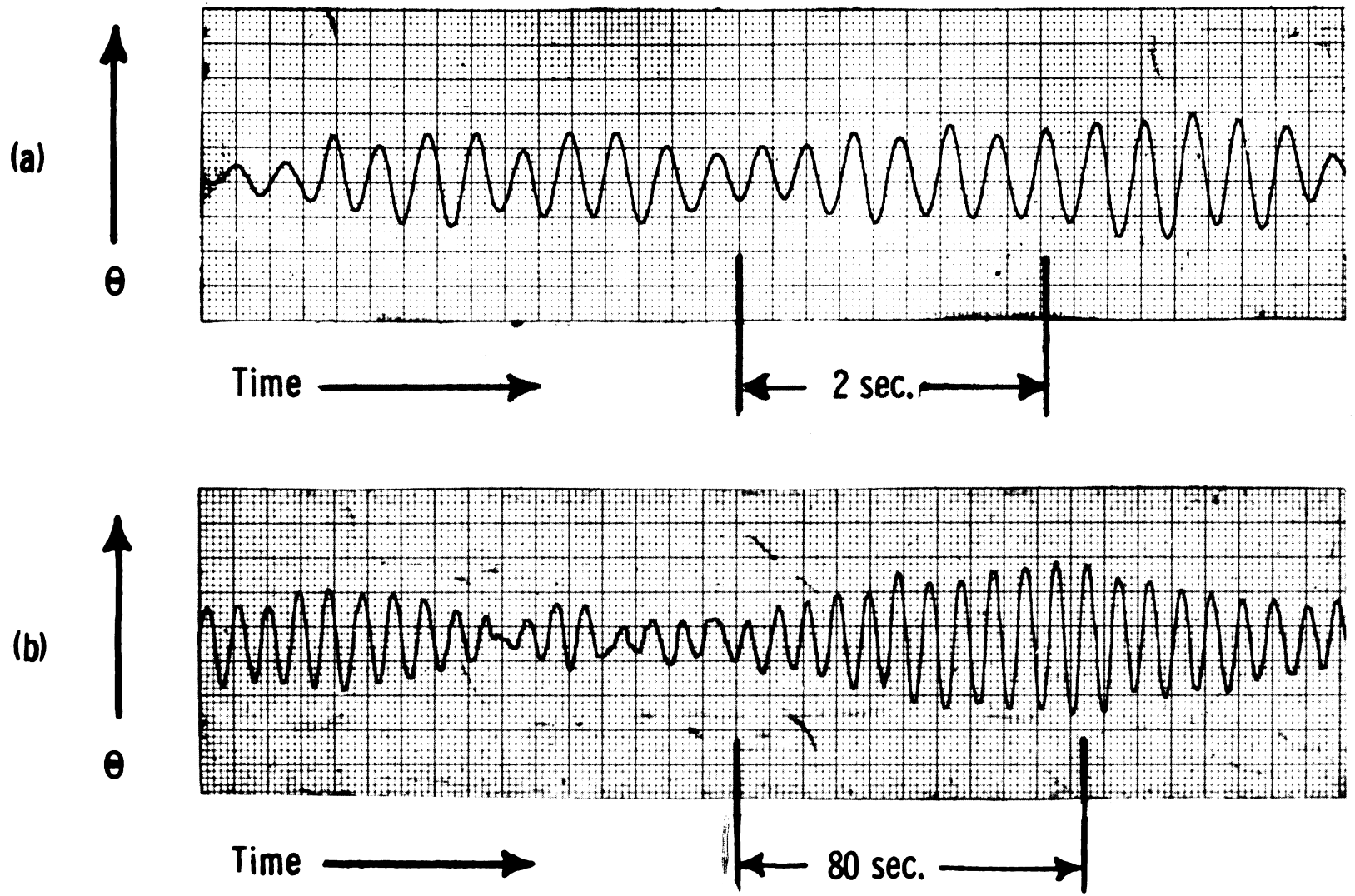

Fig. 1. Oscillograph records of disk oscillations vs. time. (a) I* = 1.125, nd/U = 0.0305, d = 12 in., h/d = 0.0104, U = 100 fps, $\sqrt{\overline{\theta^2}}$ = 0.122 rad. (b) I* = 42.3, nd/U = 0.0054, d = 6 in., h/d = 0.125, U = 100 fps, $\sqrt{\overline{\theta^2}}$ = 0.041 rad.

steady and unsteady aerodynamic moments which cause the motion. Detailed measurements of the restoring moment, damping moment, and the random unsteady moment produced by turbulence have been made and are used to compute the mean square amplitude of oscillation.

II. THEORY FOR THE DISK MOTION

The problem of the oscillating motion of the disk about a fixed axis can profitably be studied in the light of previous work on the response of mechanical or aerodynamic systems to turbulence. Lin[2] studied the motion of a pendulum immersed in a turbulent stream. Liepmann[3] has considered the force exerted on an airfoil in a turbulent stream. These problems were analyzed using the same methods that were developed for the problems of Brownian motion of a torsional balance or the response of an electrical circuit to random noise. Liepmann[4] and Fung[5] have given general discussions of these methods as used to understand the effects of turbulence on linear systems.

For the present investigation, we can write the approximate nondimensional differential equation for the disk motion as

$$I_1^* \frac{d^2\theta}{dt'^2} + C_{m_{\dot{\theta}}} \frac{d\theta}{dt'} + C_{m_\theta}\theta = C_m'(t') \qquad (1)$$

The equation and symbols are explained in detail in Appendix A. The assumptions implicit in this equation are that the unsteady aerodynamic moment acting on the disk can be separated into three independent contributions representing damping, $C_{m_{\dot{\theta}}}(d\theta/dt')$, restoring moment, $C_{m_\theta}\theta$, and turbulence, $C_m'(t')$. The damping and restoring moment are assumed to depend only on the angular velocity and position of the disk while the turbulent moments are assumed to be independent of the disk motion and attitude. In practice this means that the disk motion must be restricted to small angles and angular velocities and the turbulent motions must not be changed appreciably by the motion of the disk.

In the remainder of the report experiments will be described which are designed to determine the nature of the damping moment, restoring moment, fluctuating turbulent moment and the disk motion.

III. EXPERIMENTAL APPARATUS

The subsonic wind tunnel experiments were conducted in the low turbulence tunnel at the Aeronautical Engineering Laboratories, The University of Michigan. This closed circuit tunnel has a 5 ft by 7 ft test section with continuously variable speed up to 225 fps.

A. FREE OSCILLATION—MECHANISMS AND SENSORS

These tests all involved a single degree-of-freedom, angular motion of the disk about a vertical axis. Two methods were used to support the model in the tunnel. These were the "sting mount" and the "vertical mount" as shown in Fig. 2. In both cases the model shaft could be supported on a pair of sealed instrument bearings.*

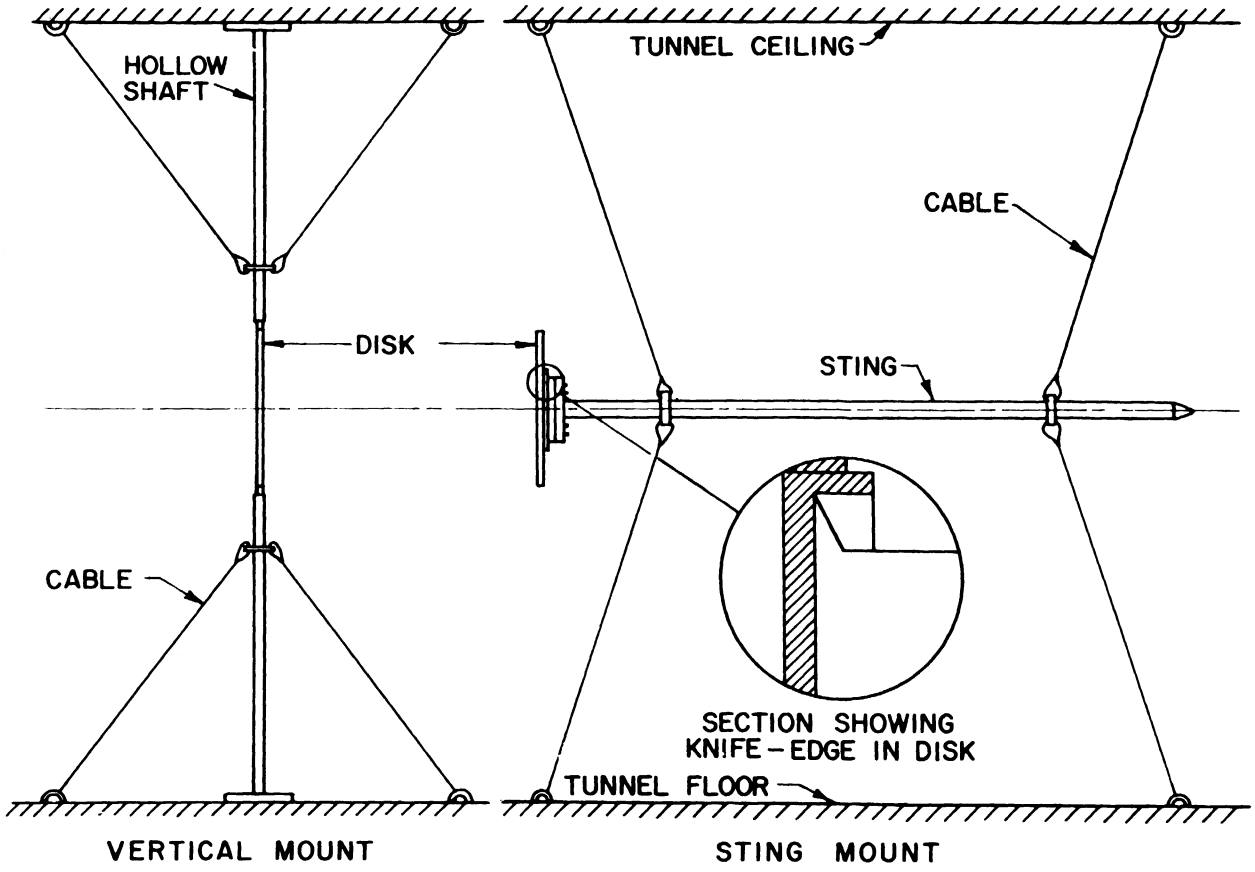

Fig. 2. Sketch showing wind tunnel mounting methods for free oscillation tests.

*Miniature Precision Bearings, Inc., Type SS614CHH.

In addition, a hardened steel knife-edge bearing could be used in conjunction with the sting mount, as depicted in Fig. 2. The knife-edge bearing gave relatively lower friction and made it possible to place the pivot line on a diameter through the center of the disk. Disks on the vertical mount were placed slightly upstream of, or exactly on, the pivot line.

In the damping tests it was necessary to displace the model to some initial angle and then release it for free oscillation. A simple piston device was placed on the sting mount to displace the model when compressed air was turned on and release it when the air was shut off. The vertical mount employed a device which engaged from the top of the tunnel through the upper portion of the hollow shaft. This enabled one to displace and release the model manually.

The two photoelectric systems which were used to obtain disk angular position vs. time are shown in Fig. 3. In the photocell system, two selenium photocells* are mounted as shown and connected electrically so as to oppose one another. If the cells are well matched and the lamp position is carefully adjusted, the voltage across the cells is quite linear with respect to angular position up to displacements of ± 20° and

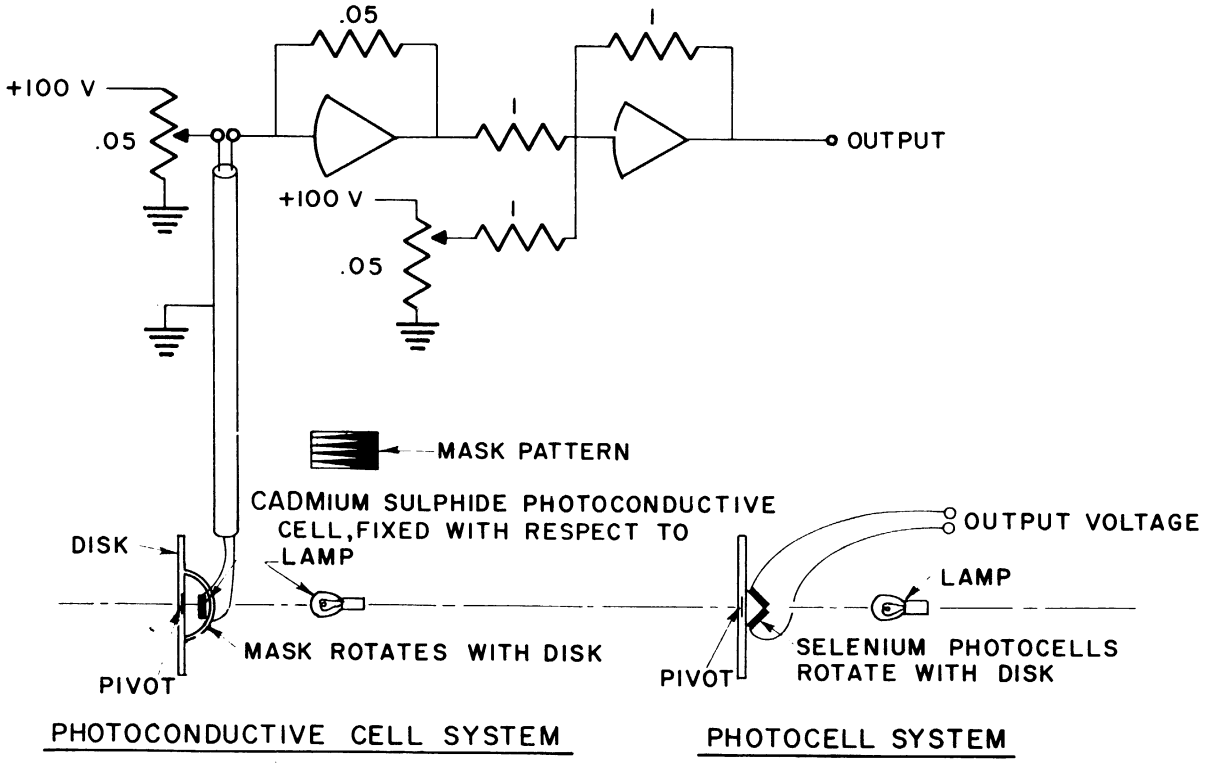

Fig. 3. Photocell and photoconductive cell angular position systems.

*International Rectifier Corporation, type B2M.

often ± 30°. A Sanborn dual channel Twin-Viso Recorder was used to record the disk motion and Fig. 4 gives a sample calibration taken on the recorder. One disadvantage of the photocell system was that the voltage was taken from the oscillating cells by means of very fine wires which were subject to frequent breakage and whose effect on the disk motion was unknown. Thus for the knife-edge bearing a new system was developed using a Cadmium sulphide photoconductive cell* in conjunction with analog computer elements. A clear Plexiglas "mask" of cylindrical shape was attached to the aft side of the disk (see Fig. 3) so that its center line coincided with the pivot line. Various methods were tried to obtain an opacity gradient along the perimeter of the mask so that as the disk oscillated, the photoconductive cell would receive varying amounts of light according to disk position. It was found that the mask pattern shown in Fig. 3 when drawn with pencil on translucent vellum paper gave satisfactory results. In this case the photoconductive cell resistance was inversely proportional to the amount of light being received. To overcome this difficulty, the cell was hooked into the analog circuit of Fig. 3 as an input impedance. As a result the first operational amplifier produced a voltage output directly proportional to the light being received and therefore proportional to disk position. The second amplifier was used to bias the voltage so that on the output zero volts corresponds to $\theta = 0$. A sample calibration of the photoconductive system is also given in Fig. 4.

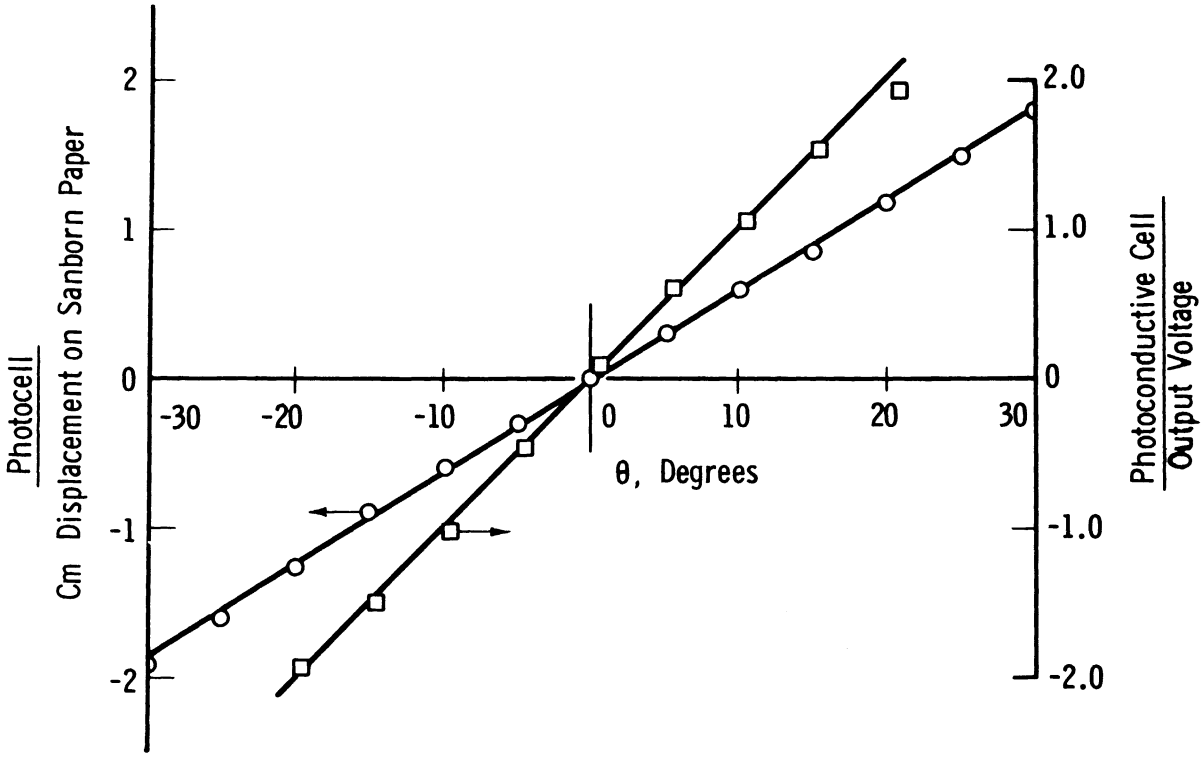

Fig. 4. Typical calibration data for the photocell and photoconductive angular position sensors.

*International Rectifier Corporation, type CS-120-M6.

The disks themselves were made of various materials ranging in density from brass to balsa wood. The diameters varied from 0.33 ft to 1.00 ft and the thickness/diameter ratios from 0.0104 to 0.1250. Two of the aluminum disks (1.00 ft and 0.50 ft diam) had hat-shaped fairings which could be attached to the aft side of the disk. These fairings could be filled with modeling clay to further increase the moment of inertia. On the 0.92 ft diam plywood disk the moment of inertia was increased by attaching steel plates to the aft side of the disk. With the exception of the balsa disks, all the disks had sharp, square edges.

B. FORCED OSCILLATION—MECHANISMS AND SENSORS

The forced oscillation mechanism is powered by a 1/2 hp electric motor driving a Vickers variable speed hydraulic transmission.* The transmission turns a large steel flywheel (0.25 slug-ft^2) to which is attached an eccentric with an adjustable radius. The eccentric in turn drives a scotch yoke which transmits its sinusoidal reciprocating motion to the model supporting shaft by means of a steel tape-pulley arrangement. Considerable care was taken in the design to assure that the resulting angular motion of the supporting shaft would not vary significantly from a sinusoid under all operating conditions.

The torque from the oscillator mechanism is applied to the lower shaft of the moment balance, which is sketched in Fig. 5. The balance consists of an outer cylindrical shell which contains an inner shaft supported by a pair of three-wire flexures. These flexures offer minimum resistance to relative rotation between shaft and shell without the disadvantages of ordinary bearings which are subject to effects of dust, corrosion, and wear. The torque which acts on the disk is carried by the model mounting beams to the inner shaft. This torque is then transmitted to the strain gage beams by the yokes and 0.015 in. steel flexure wires, and finally carried to the lower shaft by the components of the outer shell. The gage beam design required a compromise between the necessity for a high moment balance sensitivity on one hand and stiffness on the other. High sensitivity is needed to measure small aerodynamic moments accurately, and stiffness is required to prevent low frequency vibration of the disk relative to the supporting shaft. The gage beams are made from steel hardened to Rockwell C 40. The 350 ohm, epoxy backed, foil gages** are of constantan alloy compensated for steel and bonded to the metal by an epoxy heat-curing cement.*** The four gages (two gages per beam) are connected in a four arm bridge so as to provide the maximum sensitivity to torsion with minimum interaction to other loads. It was experimentally determined that the minimum readable moment on this system is of order 0.01 ft-lb. The balance was tested for interaction with the expected maximum drag load (26 lb) applied normal to the axis of rotation. The interaction was of the order of the minimum measureable moment. A typical calibration is given in Fig. 6.

*Vickers, Inc., series TR3, 3/4 hp.
**Budd Instruments Division, type C6-161-B350.
***Wm. T. Bean Co., type BAP-1.

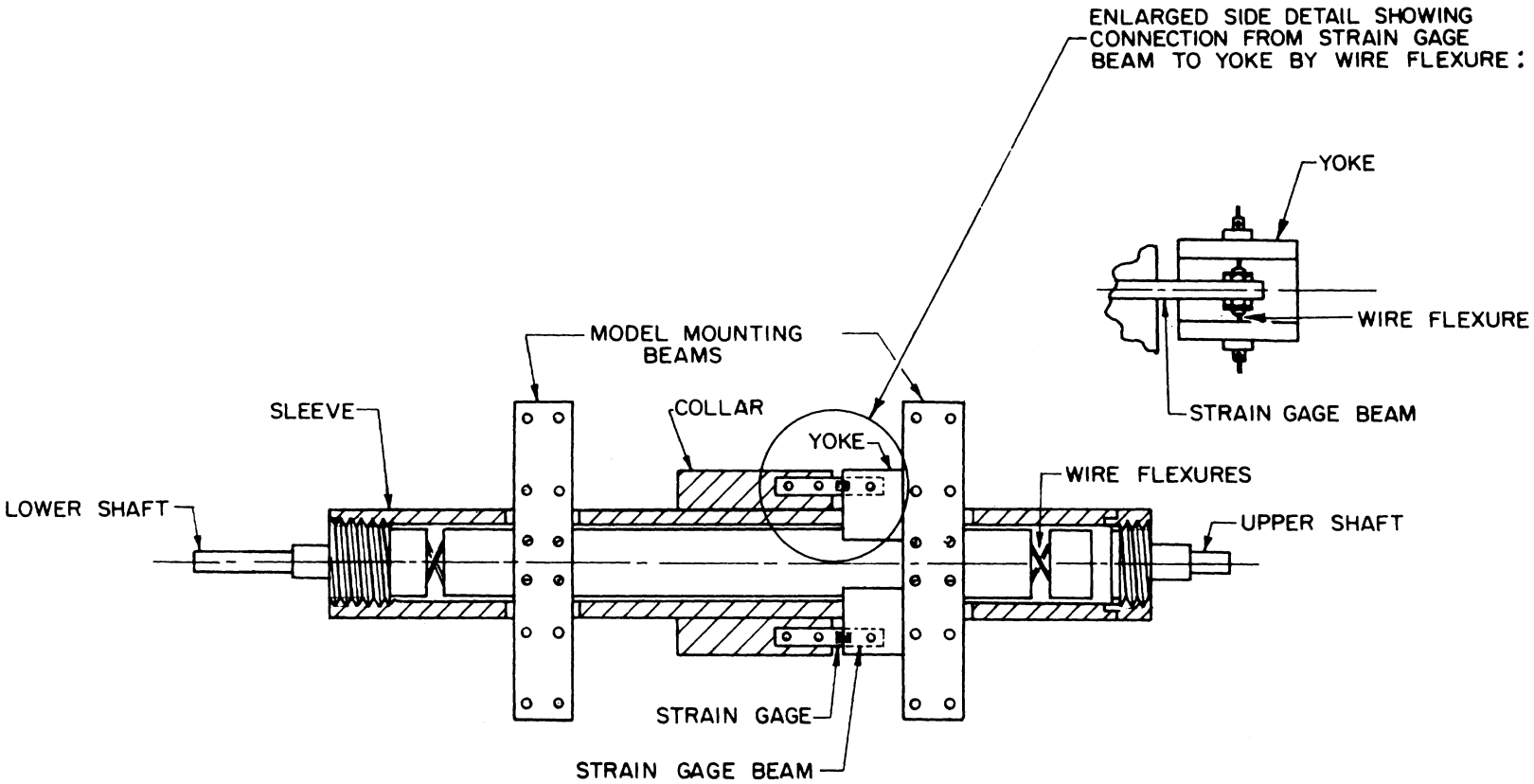

Fig. 5. Sketch showing essential components of moment balance, 1/2 scale.

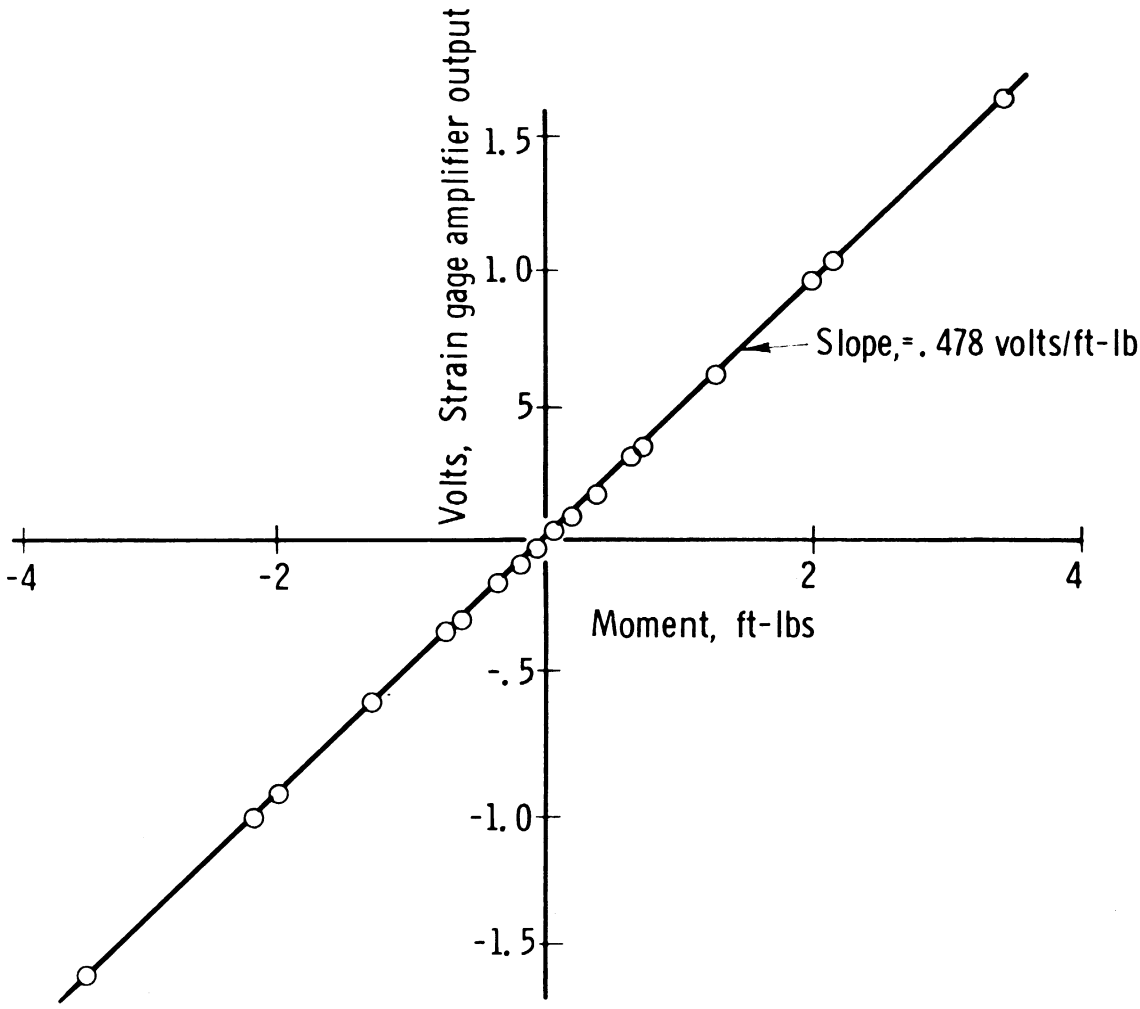

Fig. 6. Calibration of moment balance.

In order to obtain a low moment of inertia the 1.83 ft diam x .198 ft thick disk was constructed of low density Styrofoam supported internally by aluminum angles which carried the loads to the torsion balance. A low moment of inertia was desirable because (1) the inertia moment should be as low a fraction of the total moment as possible in order to measure the aerodynamic moment more accurately, and (2) a high disk inertia would lower vibration frequency between the model and supporting shaft. Figure 7 is a photograph of the Styrofoam disk in the tunnel with a plywood disk downstream. Because of the difficulty of measuring the moment of inertia experimentally, it was decided to obtain it by calculation. Each component of the disk was weighed and measured before assembly. The calculated moment of inertia is $I = 98.6 \times 10^{-4}$ slug-ft^2. The disk was made relatively thick (h/d = 0.108) in order to keep its rigidity as high as possible.

There are two electrical components directly associated with the moment balance

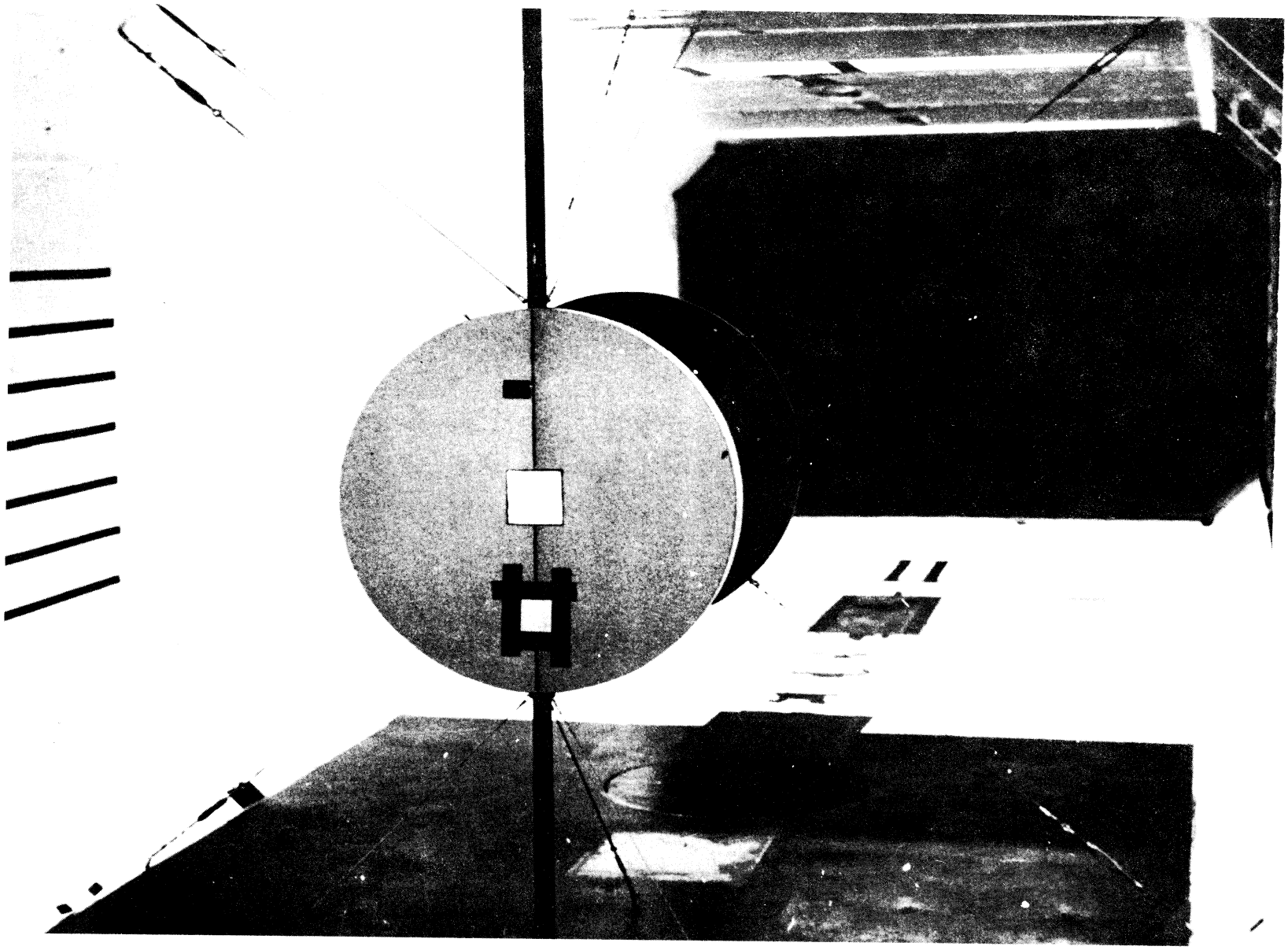

Fig. 7. d = 22 in., h = 2-3/8 in. Styrofoam disk mounted in tunnel with 22 in. diam plywood disk downstream.

and oscillator mechanism. First, the strain gage bridge is connected to a Consolidated Electrodynamics Corporation Amplifier System D. This system provides a 10 v 3 kc carrier for bridge excitation with the voltage and frequency held constant with ± 1%. The frequency response is flat from dc to 600 cps. The other electrical component is the position pot, the wiper shaft of which is attached to the oscillating model support shaft and gives an output voltage proportional to the disk position. It was found that good quality wire-wound pots were too noisy for this application. A film potentiometer* turned out to be very satisfactory for our purpose, since the voltage change as the wiper moves is continuous and noise is at a minimum. The voltage across the pot was 200 v supplied by the reference voltages in the analog computer.

C. ELECTRICAL PROCESSING, COMPUTING, AND STORAGE

There were several electronic instruments used in the course of the experiments and each is briefly described here.

1. Computer. The computer is an Applied Dynamics Model AD-1 electronic differential analyzer. The operational amplifiers of the computer have a typical drift of 1 mv/hr referred to input, ac noise normally less than 1 mv rms referred to input, and are balanced manually within ± 2 mv referred to input. The multiplier has a maximum error of 0.3 v. The input and feedback impedances are accurate to 0.02%. A total of 12 operational amplifiers and 10 coefficient potentiometers were available in our particular setup. Standard analog circuits were used and each is described in more detail in relation to individual experiments.

2. Tape Recorder. Recordings were made on an Ampex Model FR-1100 magnetic tape recorder. The recorder employs FM electronics and has frequency response from dc to 1250 cps at 7-1/2 ips tape speed. This instrument was especially useful in studying the low frequency phenomena of free oscillations. This data was recorded at 7-1/2 ips tape speed and played back at 60 ips, increasing all frequencies by eight. Hence frequencies as low as 0.025 cps could be studied by means of the wave analyzer.

3. Wave Analyzer. The low frequency wave analyzer consisting of a narrow band filter circuit with a frequency range from 0.2 to 160 cps was used to obtain all the spectral data. A thermocouple was used to measure the mean square of the analyzer output. Since the band pass was variable within limits, all data was approximately normalized to a band pass of 1 rad/sec.

4. Oscilloscope. Electrical signals were monitored with a Tektronix model 502 dual-beam oscilloscope. A Tektronix model C-12 scope camera was also used to photograph traces.

---

*Computer Instruments Corporation, No. 205.

IV. RESULTS AND DISCUSSION OF THE EXPERIMENTS

A. FREE OSCILLATIONS

The general nature of the free oscillations is indicated by the oscillograph records of the motion of Fig. 1. This motion was observed whenever the disks oscillated about their statically stable equilibrium position with face normal to the flow. Autorotation of the disks was never observed to occur when the disks and fluid were at rest and the tunnel speed was slowly increased. Autorotation was observed if the disks were given an initial angular velocity while the tunnel was running. We have studied only the free oscillations about the equilibrium position.

1. Frequency of Oscillation. The first tests showed that each disk oscillated continuously with frequency dependent on wind speed and with an amplitude and phase which appeared to vary in a random manner. Figure 1 which gives amplitude vs. time records of two disks, is typical. The average frequency of the oscillation was measured by simply counting the number of cycles in a given time. It was found that for a given model, nd/U was nearly constant, varying slightly with Reynolds number. Figure 8 gives the relation between nd/U and the reduced inertia, $I^* = I/\rho d^5$ for several disk models. As outlined in Appendix A, the dimensionless frequency, nd/U, of a second order linear system with no damping should vary as $(I^*)^{-.50}$ whereas the present result (from Fig. 8) is that the dimensionless frequency varies as $(I^*)^{-.44}$. Although sufficient damping can make the exponent less negative, these disks were far too lightly damped to account for the difference.

2. Static Restoring Moment. By clamping the Styrofoam disk at fixed angles of attack, it was possible to obtain the static restoring moment coefficient as a function of angle of attack. Because the moment fluctuated considerably due to random disturbances, it was necessary to electrically integrate the output of the strain gage amplifier with analog components and divide by the time of integration to obtain an average restoring moment. The resulting data is given in Fig. 9. It can be seen that there is a difference between the data at high and low Reynolds numbers. The restoring moment coefficients at $\theta = 0$ were $C_{m\theta} = 0.126$ per rad at the lower Reynolds number and $C_{m\theta} = 0.161$ per rad at the two higher Reynolds numbers. This same effect has been inferred in free oscillation tests where the dimensionless frequency increased slightly with Reynolds number. For example, one test of a 1.0 ft aluminum disk showed the calculated $C_{m\theta}$ changing from 0.114 per rad to 0.130 per rad as the Reynolds number increased from 3.61×10^5 to 5.61×10^5. Hence we have the same trend from frequency measurements in free oscillation and static measurements of $C_{m\theta}$. The lower values of $C_{m\theta}$ determined from the free oscillation measurements are probably (as the static measurements show) caused by the decrease of $C_{m\theta}$ when θ increases.

3. Damping of Free Oscillations. The linear theory for disk oscillations outlined in Appendix A predicts that the rate of decay of the motion is simply related to the amount of damping when turbulent exciting forces are small. The determination of the damping from the free oscillation records of disks that were displaced and re-

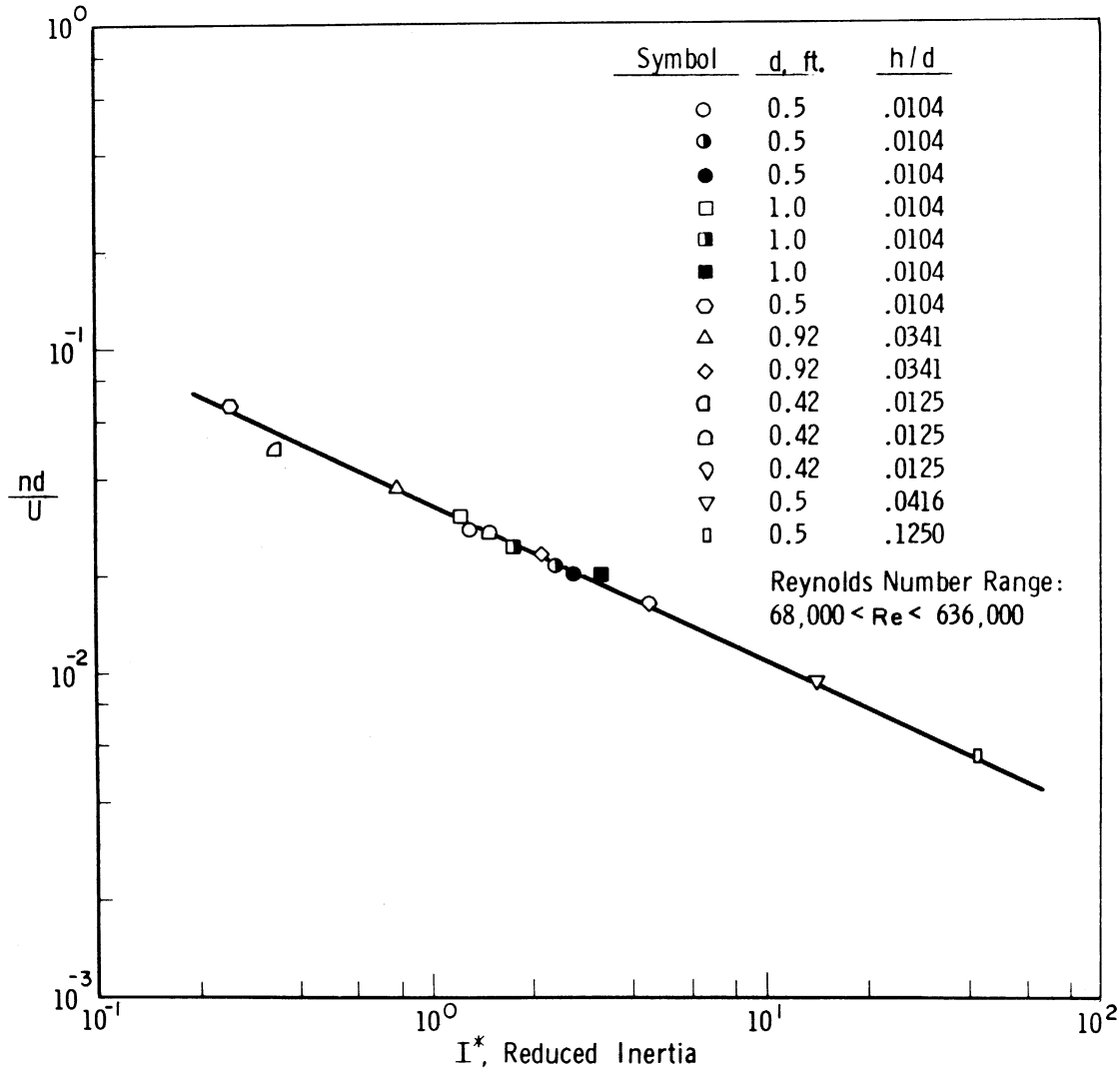

Fig. 8. Reduced frequency, nd/U, vs. reduced inertia, I*, for free oscillation.

leased was severely hampered by the random fluctuations which occurred during the damped motion. A large number of amplitude vs. time records were taken after release of the disk from an angular displacement varying from 20° to 40°. The theoretical dependence of $C_{m\dot{\theta}}$ on the damped motion is (see Appendix A),

$$\log \frac{\theta_o(t)}{\theta_o(o)} = - C_{m\dot{\theta}} (\log e) \left(\frac{\pi^2}{8}\right) \left(\frac{N}{I^* \omega^*}\right) \qquad (2)$$

where $N = \omega t/2\pi$ is the total number of cycles which have elapsed after the release of the disk from its initial position and $\theta_o(t)$ is the amplitude of the motion. When

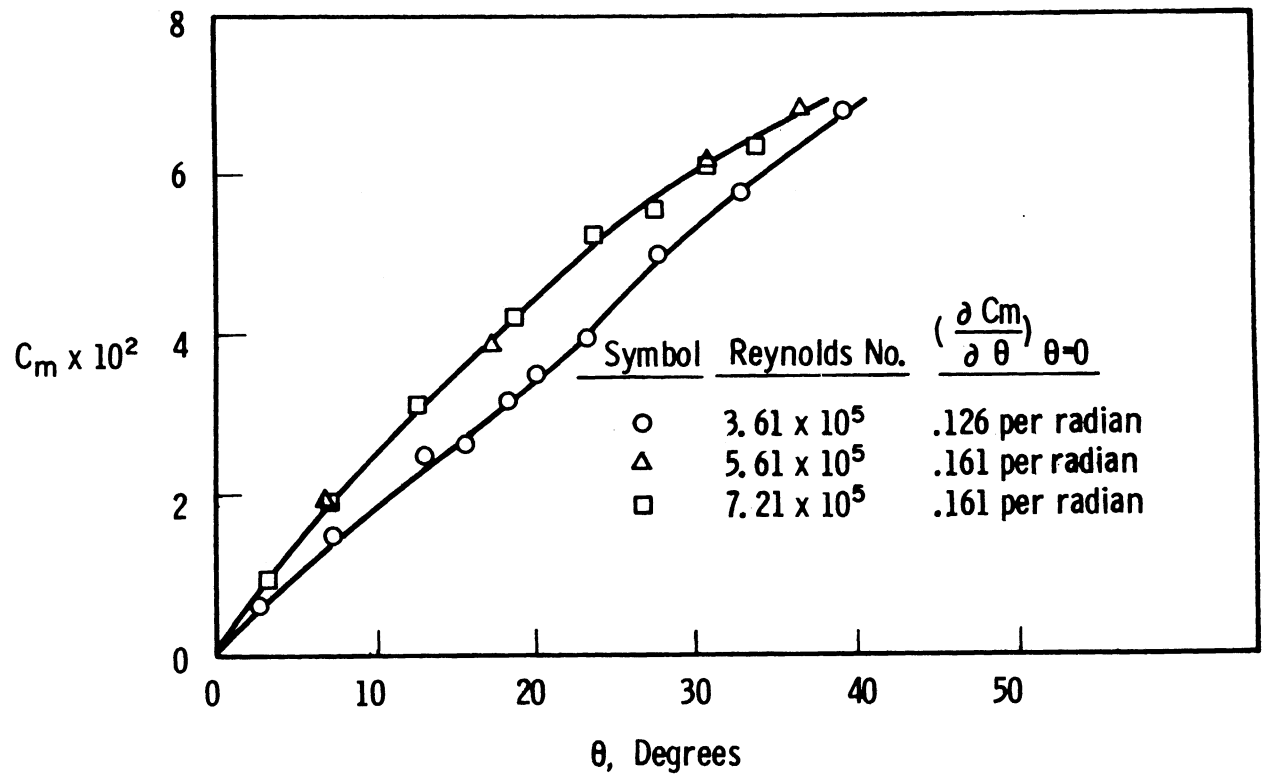

Fig. 9. Static moment coefficient, C_m, vs. disk deflection angle, θ, Styrofoam disk, d = 22 in., h = 2-3/8 in.

log $\theta_o(t)/\theta_o(o)$ is plotted against $N/I^*\omega^*$, all configurations which have the same $C_{m\dot{\theta}}$ should follow a single straight line.

The very large amount of scatter present in the original data was reduced by averaging the damping data for each individual disk, and the result is shown in Fig. 10. The damping coefficients which can be measured from slopes taken from point-to-point on Fig. 10 vary from 0.025 to 0.07. The dashed line indicates an overall average damping factor for all the configurations of $C_{m\dot{\theta}} = 0.040$. It does not seem possible, because of the wide scatter, to accurately determine the damping coefficients of the disk from these tests.

4. Statistical Analysis of Free Oscillations. The records of the disk motion were analyzed statistically to determine the nature of the random oscillations and to determine the relationship of the disk motion to the unsteady aerodynamic phenomena that cause the motion.

Records of the disk motion were obtained from electrical signals produced by photoelectric and photoconductive devices illuminated by light whose intensity was modulated by the disk motion (see Fig. 3). The signals were recorded by an oscillo-

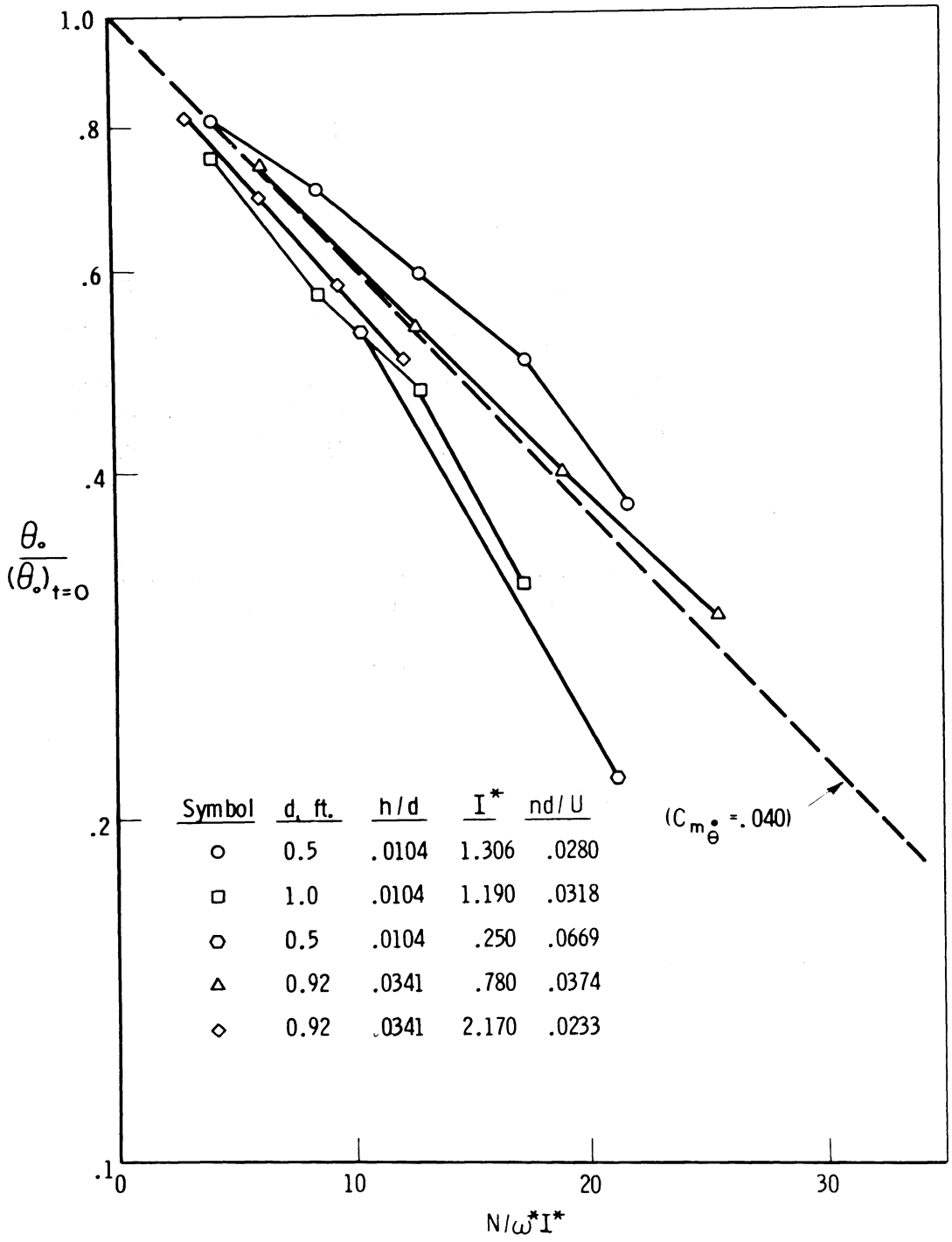

Fig. 10. Average damping for several disks in free oscillation after release from an initial angle.

graph and a frequency modulated magnetic tape recorder. Some of the motions contained very low frequency fluctuations which were recorded at low tape speeds, 7-1/2 ips, and were later reproduced at 60 ips tape speed thereby increasing the frequency by a factor of eight.

The probability distributions of motion of a number of disks of various inertia and at various wind speeds were determined using analog computer circuits (see Figs. 11 and 12). The mean square amplitude of the disk motion was determined with the analog computer and was used to normalize the probability distribution for each disk.

The probability distributions for six disks are shown in Figs. 11 and 12. It is apparent that the distribution is approximately Gaussian (see Ref. 6),

$$P(\theta) = \frac{1}{\sqrt{2\pi}} \int_{-\infty}^{\theta/\sqrt{\overline{\theta^2}}} e^{-\gamma^2/2} d\gamma \quad . \tag{3}$$

However there are deviations from the Gaussian distribution for both small and large amplitudes. The damping introduced by the type of pivot used to support the disk has a large effect on the root mean square amplitude of the motion. The best pivot was a knife edge (see Fig. 12). Higher root mean square amplitudes were obtained with this pivot than with the best ball bearings we could obtain. In fact, two tests with a knife edge and ball bearing pivot on the same aluminum disk at the same wind tunnel conditions showed that the root mean square amplitude was 50% greater with a knife edge pivot. One can appreciate that the damping forces must be extremely small. Tests with thick heavy brass disks showed very small root mean square amplitudes. The tables on Figs. 11 and 12 give the results of some of the root mean square amplitude measurements.

Close examination of the probability distribution function for the disk with the knife-edge pivot shows that the large amplitude oscillations are slightly less probable than one would expect if the random motion was a Gaussian process. We do not know whether the exciting moment and/or nonlinearities in the governing differential equation are responsible for the deviation from the Gaussian distribution. When the disks were heavy and the bearing damping reduced the amplitude of oscillation the distribution was also not Gaussian but in this case large amplitude motions became more probable and small amplitude motions less probable than one would expect for a Gaussian process. These deviations from the Gaussian process do not appear great enough to warrant further investigation at this time when we are trying to understand only the gross properties of the disk motion and aerodynamic phenomena.

A question that arose early in the investigation was: How can one decide whether the disk motion is influenced by flow fluctuations upstream of the disk? In an attempt to determine the source of the unsteady moments that cause the motion a number of different tests were made. We will discuss the tests that involve statistical observations of the motion of the disk (output of the system) in this section

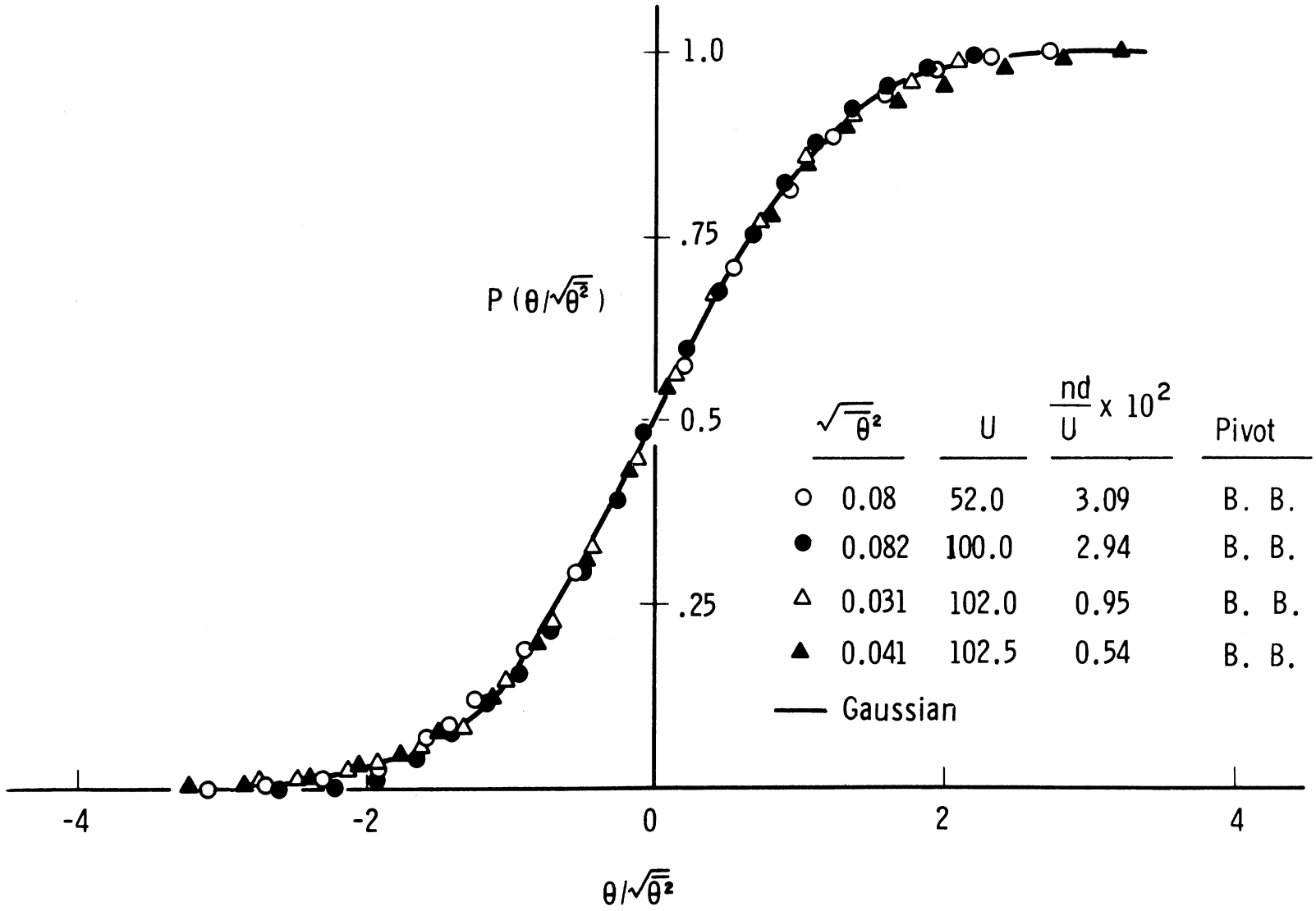

Fig. 11. Comparison of the probability distribution of disk oscillations with the Gaussian distribution (ball bearing pivot).

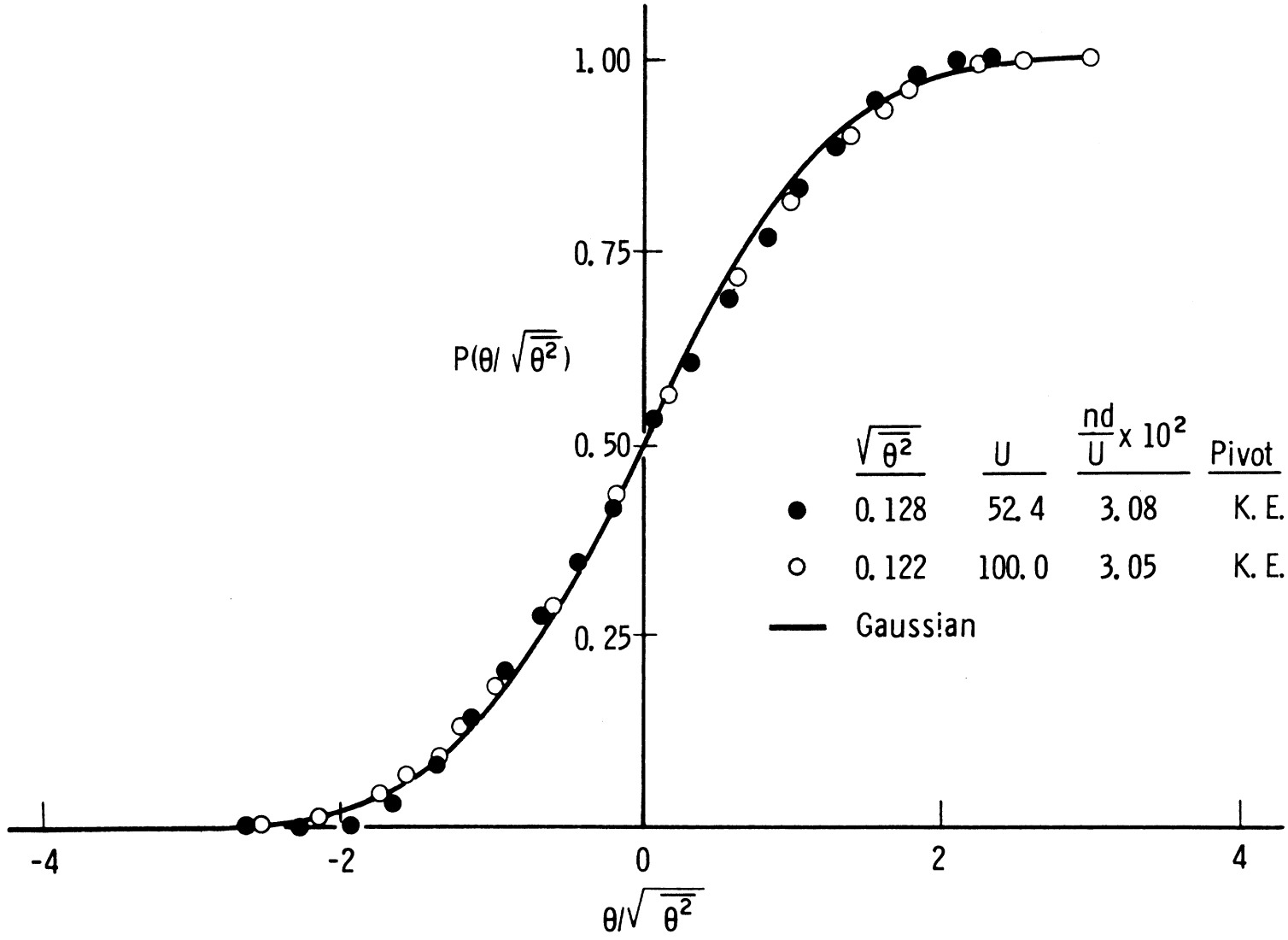

Fig. 12. Comparison of the probability distribution of disk oscillations with the Gaussian distribution (knife-edge pivot).

and reserve a description of the direct measurements of the unsteady aerodynamic moment (input of the system) and the computation of the root mean square amplitude of oscillation until Section IV-B, 4 and 5.

The records of the motion of the disk suggested that statistical measurements of the random variation of the amplitude of disk oscillations might provide information about the exciting forces if the aerodynamic parameters and disk diameter were varied. We took oscillograph and magnetic tape records of the motion of a number of disks at various wind tunnel speeds and analyzed the probability density of the slowly varying amplitude of oscillation $\theta_o(t)$ where

$$\theta(t) = \theta_o(t) \cos [\omega t + \phi(t)] \tag{4}$$

Here $\theta_o(t)$ and $\phi(t)$ are assumed to vary slowly compared to ωt. We analyzed the oscillograph records of the amplitude at the suggestion of Mr. T. Ishii, and determined the average amplitude of the envelope

$$\bar{\theta}_o = \frac{1}{T}\int_0^T \theta_o(t)dt \tag{5}$$

and the probability density of the envelope amplitude,

$$\frac{dP}{d\theta_o} d\theta_o = \text{Probability that the envelope amplitude is between } \theta_o \text{ and } \theta_o + d\theta_o$$

by simply taking the average envelope amplitude with a planimeter and determining density distribution by counting the number of times a peak fell within a given range of amplitudes. This procedure was rather tedious. The analog computer was then used to determine the amplitude of the envelope, $\theta_o(t)$. The sinusoidal signal was passed through a second order filter (see Fig. 13) whose damping and frequency of resonance oscillation could be varied. By adjusting the filter by trial and error and comparing the filter output with the input signal an acceptable reproduction of the function $\theta_o(t)$ was obtained (see Fig. 14). The probability distribution of the signal representing $\theta_o(t)$ was then obtained using the circuit of Fig. 15(b). The results of these measurements are shown in Figs. 16 and 17.

Figure 17 shows the directly determined probability distribution function of an aluminum disk mounted on a knife edge. This disk oscillated with the largest root mean square amplitude and represents our best case of the free oscillation of the disk. The measurements of the probability distribution of $\theta_o(t)$ can be compared with the Rayleigh distribution function

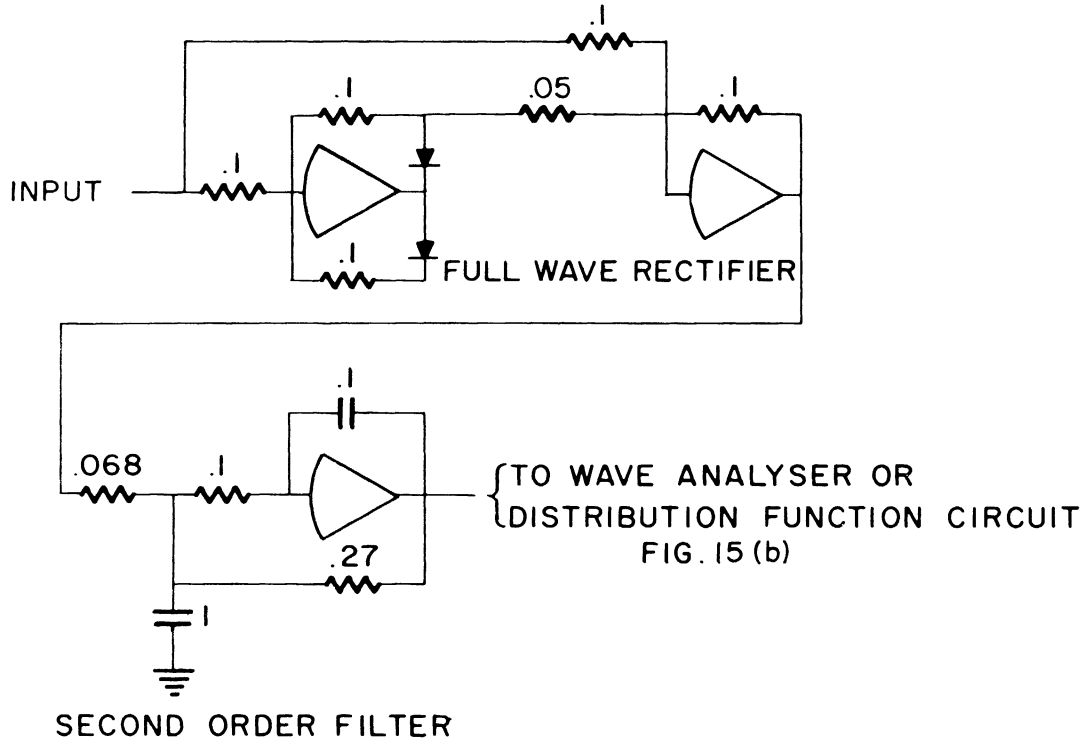

Fig. 13. Analog computer circuit used to obtain the envelope, θ_o, of the disk oscillations.

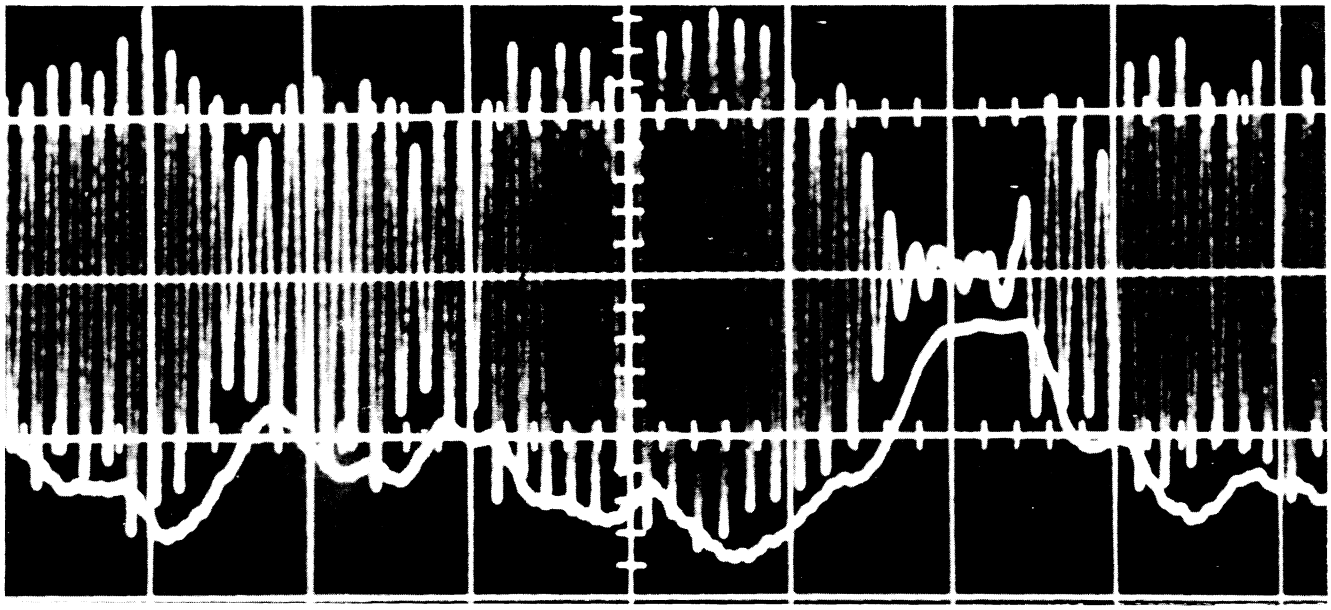

Fig. 14. Oscilloscope traces of the input and output of the envelope circuit shown simultaneously.

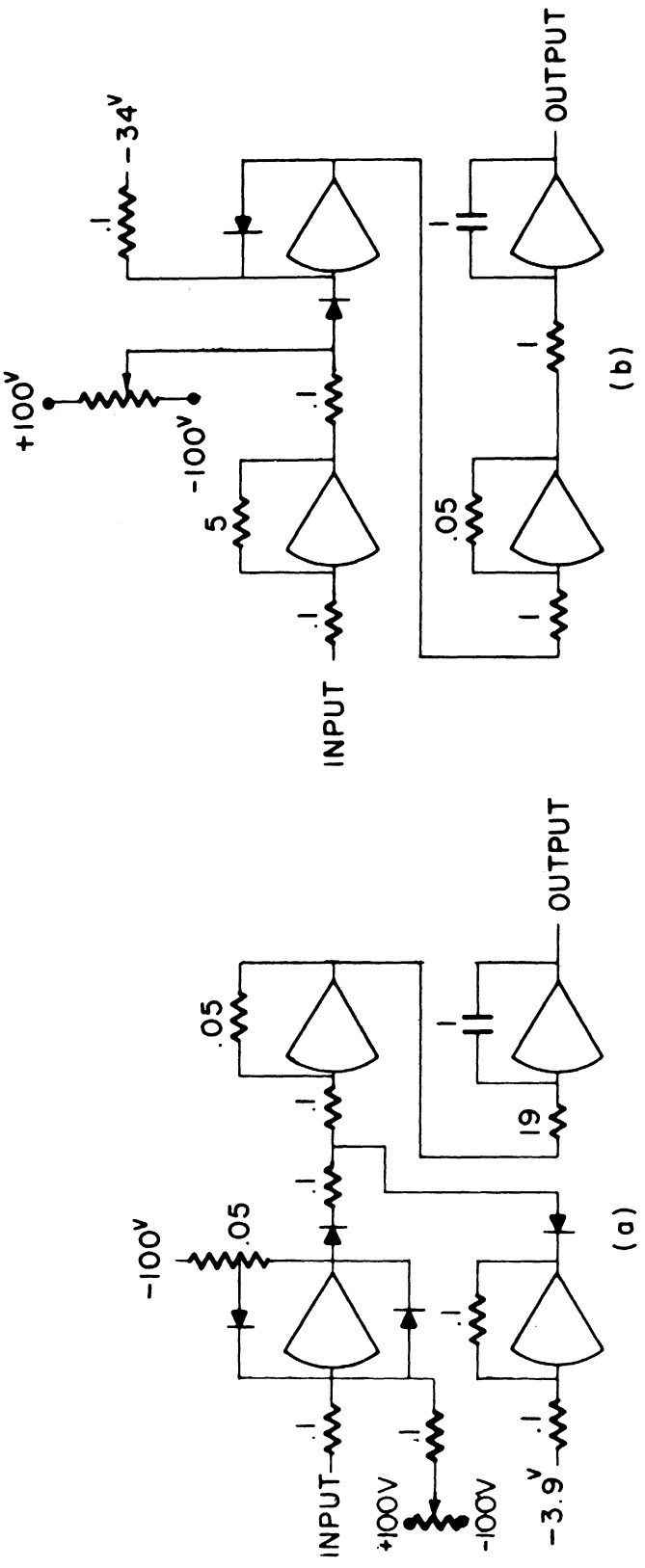

Fig. 15. Analog computer circuits for determination of the probability distribution. (a) fast recovery circuit; (b) slow recovery circuit.

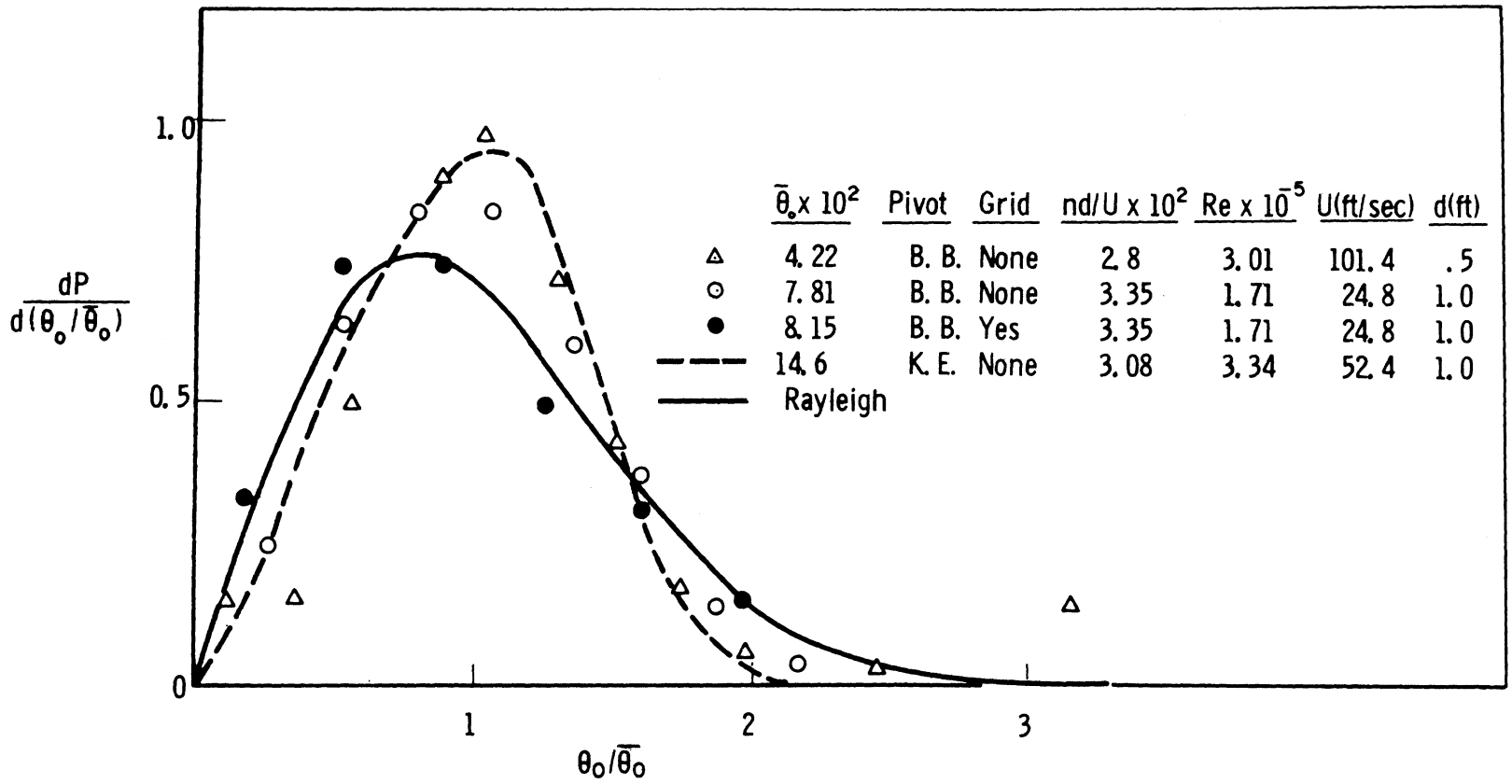

Fig. 16. Comparison between the normalized probability densities of the envelope of the disk oscillations.

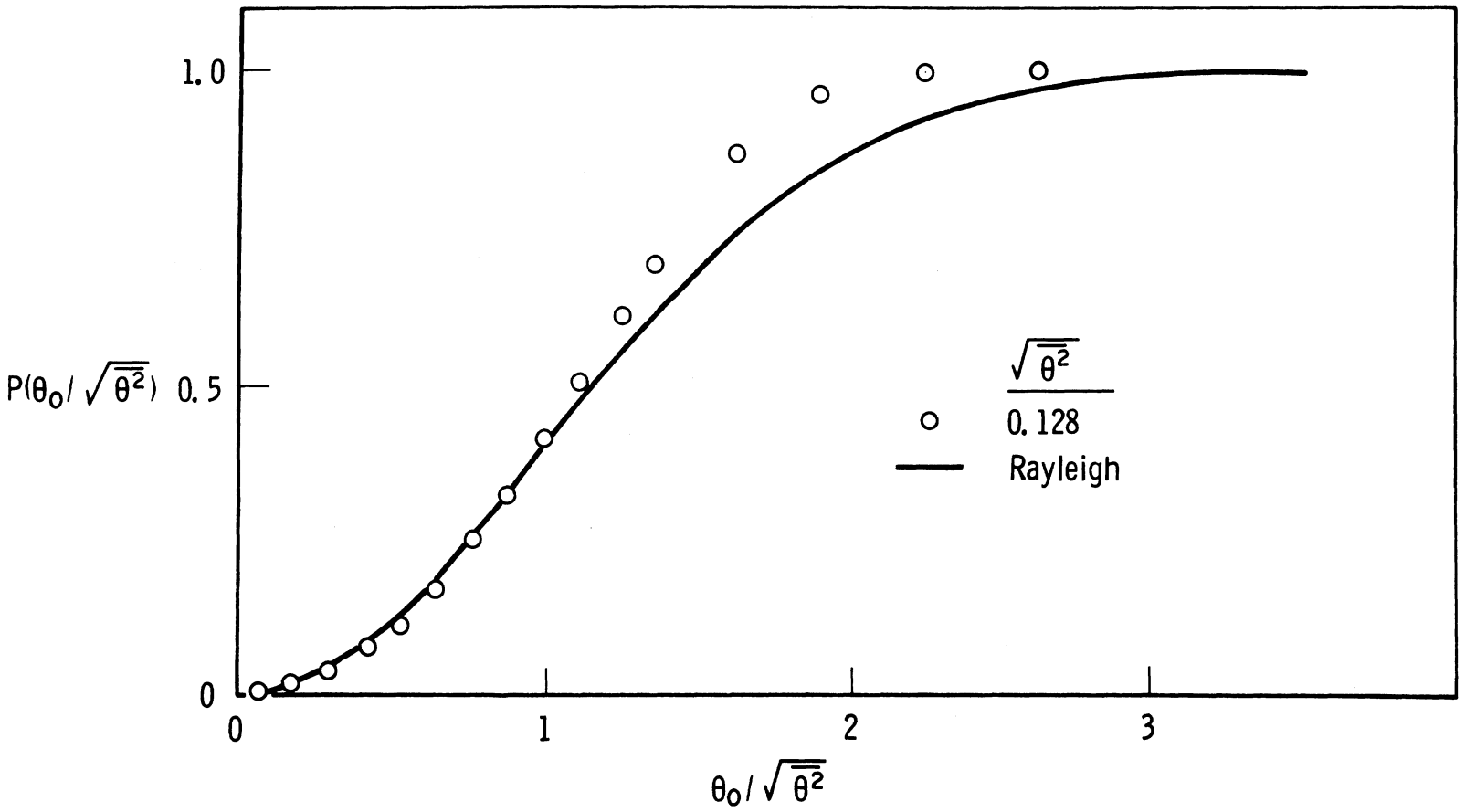

Fig. 17. Probability distribution of the envelope amplitude, Θ_o, for oscillations of a disk with a knife-edge pivot, Run 3 of Table I.

$$\text{Probability of a larger value of } \frac{\theta_o}{\sqrt{\overline{\theta_o^2}}} = 1 - e^{-\theta_o^2/2\overline{\theta_o^2}} \tag{6}$$

(see Ref. 6), which represents the probability distribution of the output of a narrow band linear system subjected to a random Gaussian input. As before, the probability distribution of the disk angle, $\theta(t)$, is different from the Rayleigh distribution which should result from a Gaussian process and again large amplitudes are suppressed.

In order to compare our measurements done with the analog computer in which $\overline{\theta^2}$ was measured, with those taken by hand in which $\overline{\theta}_o$ was measured, we have normalized the data using the mean amplitude of the envelope, $\overline{\theta}_o$, and have recast the Rayleigh probability density function Eq. (6) in the form

$$\frac{dP}{d(\theta_o/\overline{\theta}_o)} = \frac{2}{\pi}\frac{\theta_o}{\overline{\theta}_o} e^{-\frac{\pi}{4}\left(\frac{\theta}{\overline{\theta}_o}\right)^2} \tag{7}$$

using the fact that

$$\overline{\theta}_o = \sqrt{\pi/2}\sqrt{\overline{\theta^2}} \tag{8}$$

The comparison between the measurements is shown in Fig. 16 and it is clear that the measured probability density functions agree with each other but not with the Rayleigh distribution.

One test was made with a 5 ft x 7 ft turbulence grid installed in the tunnel ahead of the model. The grid was made from wooden dowels 1/4 in. in diam on center lines spaced 1-1/4 in. apart. The grid was placed 87 in. upstream of the disk. The average amplitude of oscillation was not appreciably affected by the grid but the probability density of the envelope amplitude, θ_o, was altered. The results of the probability density distribution measurement for this case are also shown in Fig. 16. The probability density is approximately the same as the Rayleigh probability density. We may say that the exciting moment acting on the disk has been altered by the grid in such a way that the mean amplitude of the envelope is not changed but larger values of θ_o are more probable while intermediate values of θ_o are less probable.

Further considerations of the nature of the exciting moment acting on the disk were clearly necessary. At the suggestion of Professor M. S. Uberoi, we measured the power spectral density of the envelope amplitude, $\theta_o(t)$, for a number of disks when no grid was installed in the tunnel. The results of the measurements were approximately corrected for variable band width, normalized, and plotted in nondimensional form in Fig. 18. The spectral density in this figure is defined by

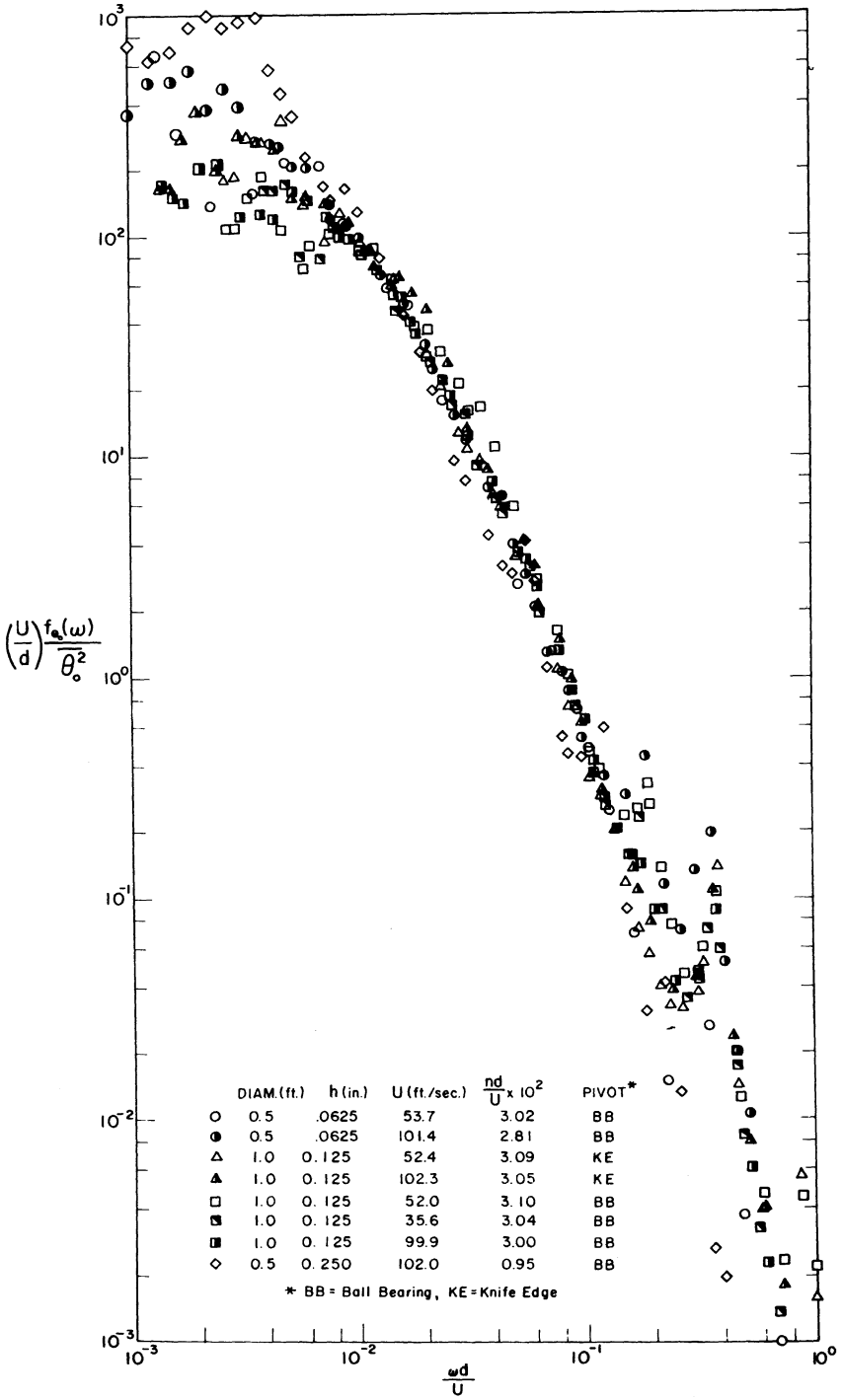

Fig. 18. Power spectra of the envelope amplitude, θ_o, for several disks in free oscillation.

$$f_{\theta_o}(\omega) = \frac{2}{\pi}\int_0^\infty \overline{\theta_o(t)\theta_o(t+\tau)}\cos\omega\tau d\tau \qquad (9)$$

The data show that the power spectra of θ_o, which must depend on the power spectra of the exciting moment, scales with the characteristic time, d/U. The spectra show considerable scatter at low frequencies but this may be the result of insufficient averaging time. The lowest frequencies (in real time) were of the order of 0.02 cps.

The important fact that the power spectra of θ_o depend on the diameter, d, of the disk and not on simply 1/U means that the wind tunnel turbulence, which should have a fixed scale, does not appreciably affect the disk motion. The wind tunnel turbulence level is

$$\frac{\sqrt{\overline{u^2}}}{U} \doteq 0.02\% \quad \text{and} \quad \frac{\sqrt{\overline{v^2}}}{U} = \frac{\sqrt{\overline{w^2}}}{U} \doteq .06\%$$

at U = 100 fps. At lower speeds the tunnel turbulence is reduced.

The result that the exciting moment for disk motion scales with the disk diameter means that the exciting moment is produced by turbulence in the disk wake which must have a length scale dependent on the disk diameter. We note that ordinary turbulence levels in the tunnel do not affect the disk motion but more severe turbulence produced behind a grid had a marked effect on the probability density of the disk motion. The model for the disk exciting moment appears to be an unsteady torque produced by wake turbulence whose statistical properties but not intensity (in this one case) can be altered by intense small scale turbulence originating upstream.

B. FORCED OSCILLATIONS

The variation of C_{m_θ} with angle and the scatter in the measurements of the damped motion made accurate determination of $C_{m_{\dot\theta}}$ from records of the motion impossible, and led us to a study of the instantaneous moment acting on a disk during forced sinusoidal motion. We designed and built equipment to produce sinusoidal motion and to study the aerodynamic moment.

1. Average Moment and Work Rate. A block diagram of the basic experimental arrangement for forced oscillation is shown in Fig. 19. The object of the apparatus is to determine the total energy dissipation over a length of time and also to give instantaneous records of aerodynamic moment, M, acting on the disk and the rate of work done on the disk by the moment, $M\dot\theta$. Typical oscilloscope traces of aerodynamic moment are shown in Fig. 20. These traces show the relatively large effect of random disturbances and vibration over a single cycle. Figure 21 gives the detailed analog circuits used to determine the average instantaneous moment and work rate. The sample and hold circuit was used to obtain an average aerodynamic torque or work rate

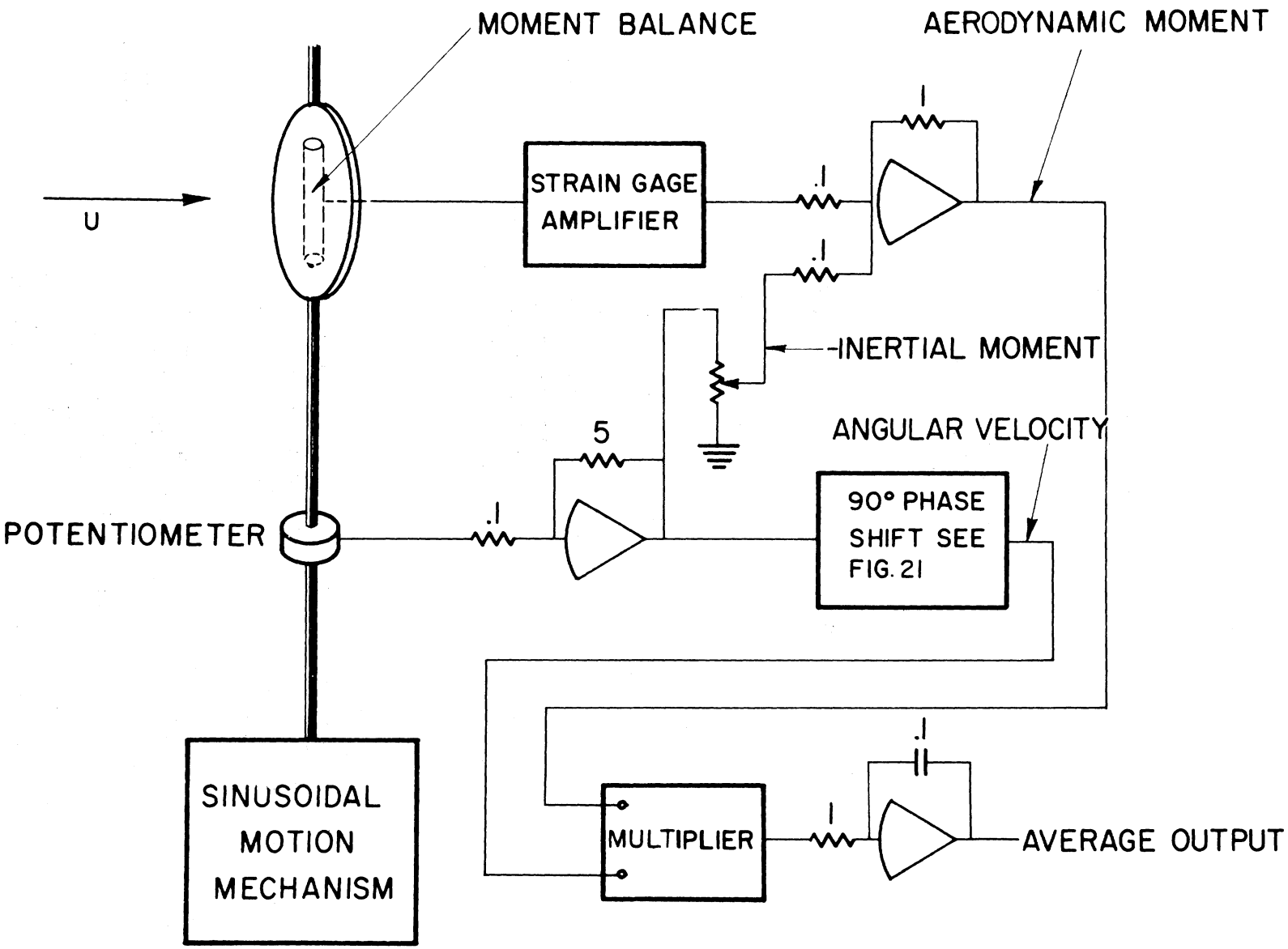

Fig. 19. Schematic diagram of experimental apparatus for forced oscillations of the disk.

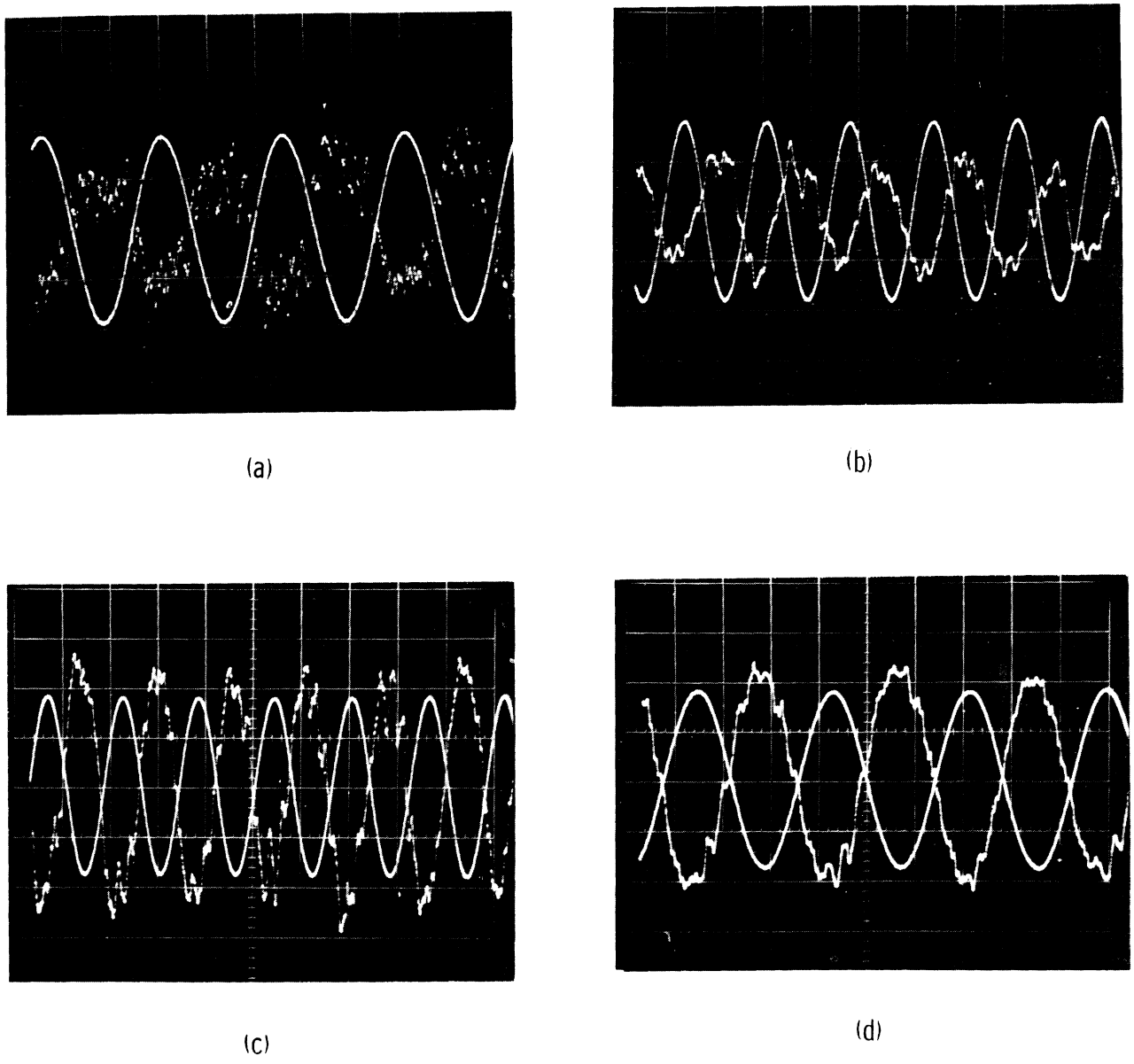

Fig. 20. Oscilloscope traces of Θ and the fluctuating aerodynamic moment acting on a Styrofoam disk. (a) Test conditions of Fig. 22; (b) Test conditions of Fig. 23; (c) Test conditions of Fig. 24; and (d) Test conditions of Fig. 25.

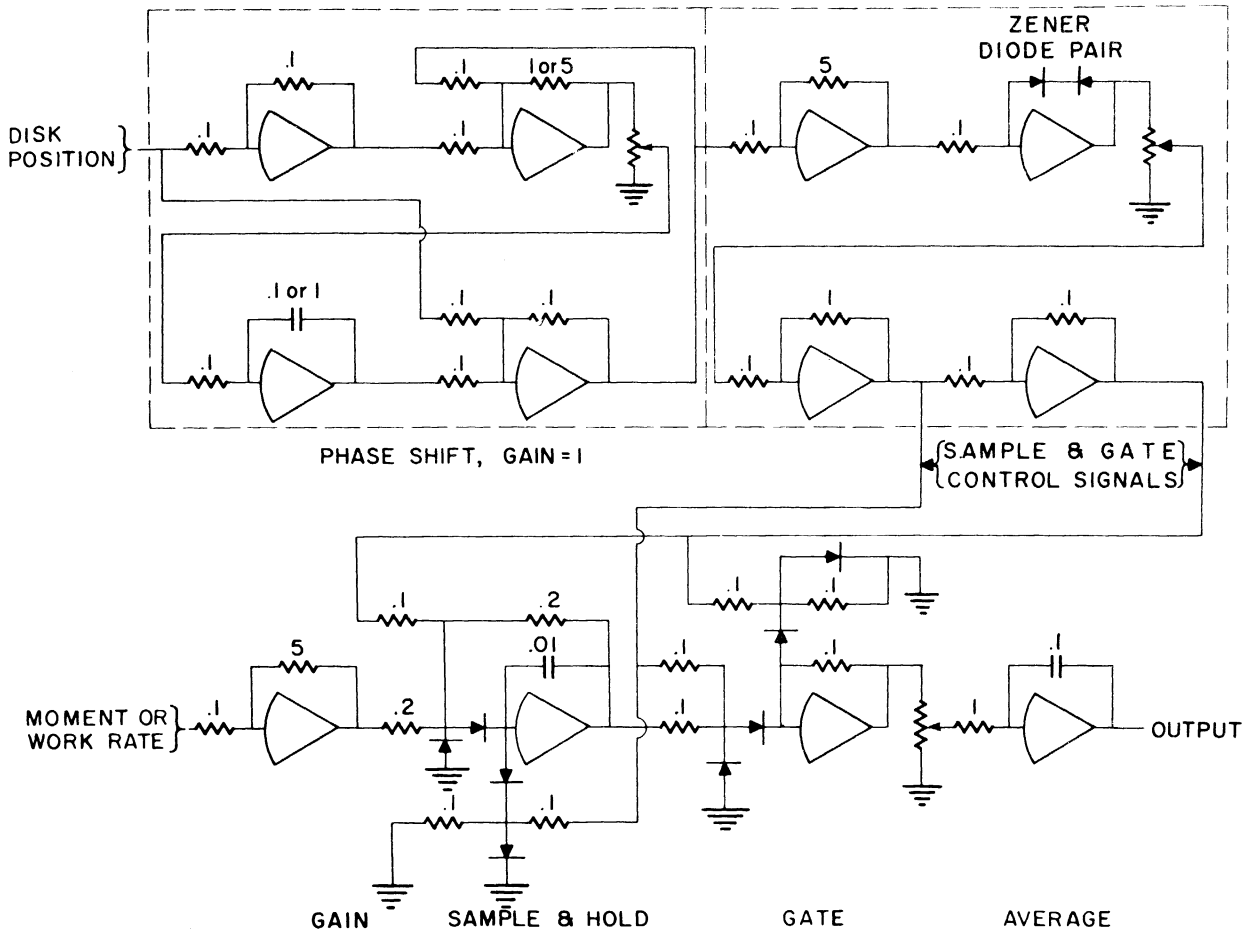

Fig. 21. Circuit for obtaining average moment or work rate as a function of time delay.

at some specific time delay after the start ($\theta = 0$) of the oscillation cycle. This was done in the following manner: The phase shifter was adjusted to some desired phase shift which determines the time delay at which the sampling is done. At that point the circuit electrically samples the voltage to be averaged and holds it for half a cycle, then follows the voltage until the same point is reached in the next cycle. The circuit again samples and holds the new voltage, etc. If the output of the sample-and-hold circuit is fed to an integrator during the half-cycle holding time and the integrator output is divided by time, the average voltage (representing average torque or work rate) is obtained for a specific time delay. This procedure was followed for four different cases of forced oscillation and the results are presented in Figs. 22 through 25 in coefficient form. Here we define

$$C_m = \frac{M}{qSd} \qquad C_{\dot{W}} = \frac{M\dot{\theta}}{qUS} \tag{10}$$

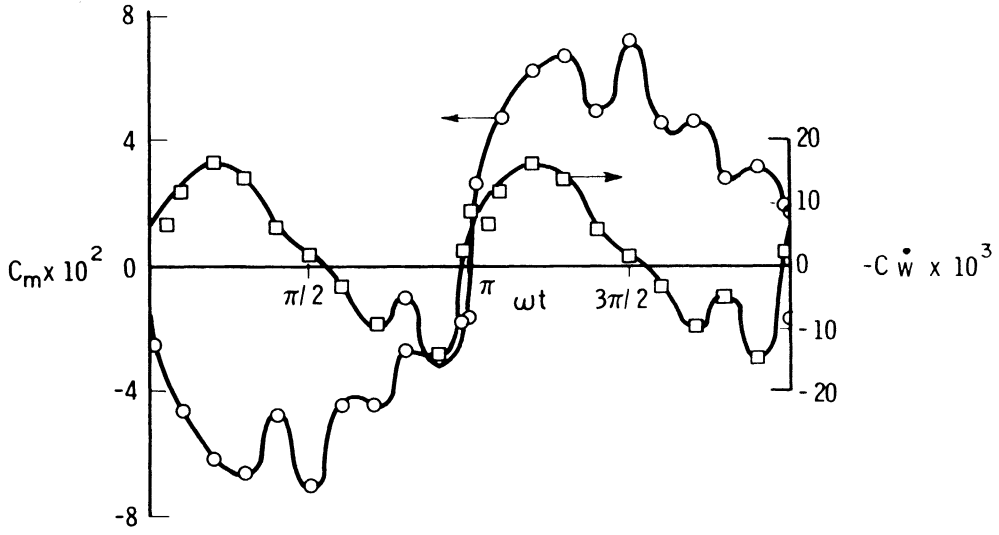

Fig. 22. Aerodynamic moment and work rate coefficients during one cycle of forced oscillation of a Styrofoam disk, d = 22 in., h = 2-3/8 in., Θ_o = 0.707 rad, ω = 12.7 rad/sec, U = 48.4 fps, Re = 5.40 x 10^5, nd/U = 7.66 x 10^{-2}.

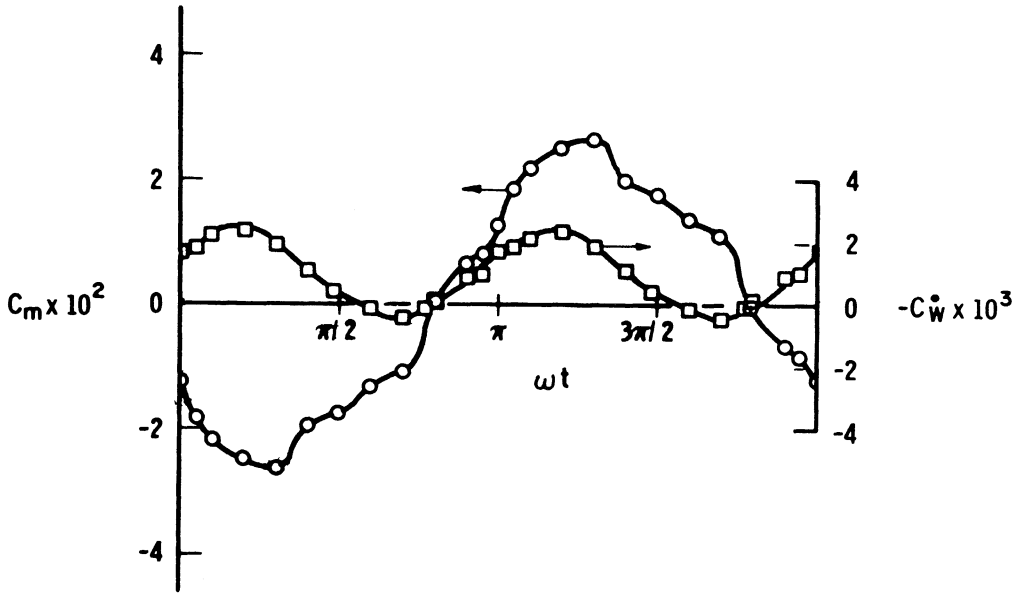

Fig. 23. Aerodynamic moment and work rate coefficients during one cycle of forced oscillation of a Styrofoam disk, d = 22 in., h = 2-3/8 in., Θ_o = 0.147 rad, ω = 37.1 rad/sec, U = 94.5 fps, Re = 10.0 x 10^5, nd/U = 11.42 x 10^{-2}.

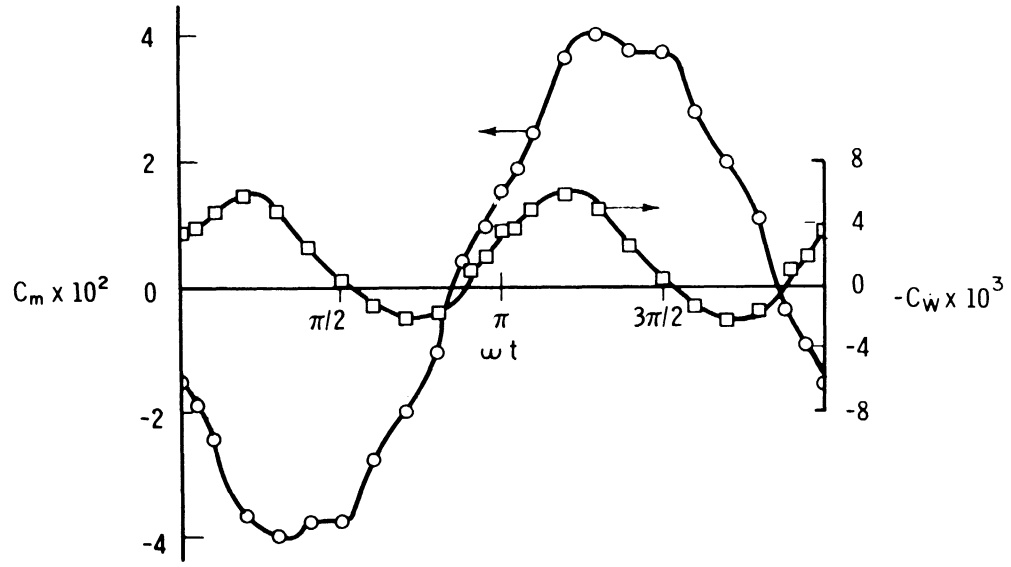

Fig. 24. Aerodynamic moment and work rate coefficients during one cycle of forced oscillation of a Styrofoam disk, d = 22 in., h = 2-3/8 in., θ_o = 0.425 rad, ω = 20.6 rad/sec U = 95 fps, Re = 9.96 x 10^5, nd/U = 6.32 x 10^{-2}.

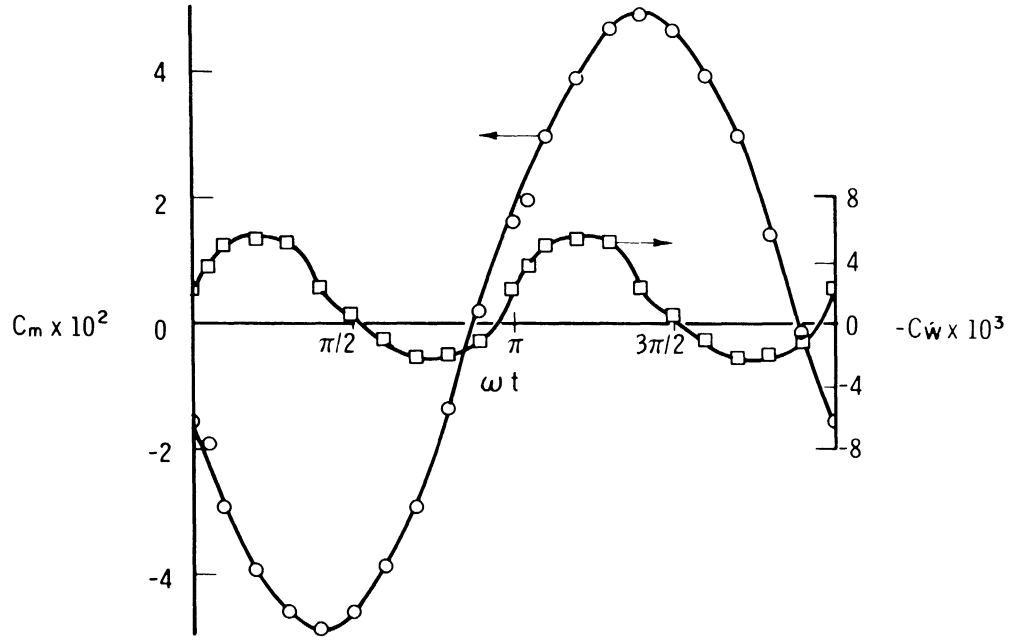

Fig. 25. Aerodynamic moment and work rate coefficients during one cycle of forced oscillation, d = 22 in., h = 2-3/8 in. Styrofoam disk with d = 26 in., h = 1/16 in. cardboard disk mounted on upstream side. θ_o = 0.425 rad, ω = 11.3 rad/sec, U = 65.4 fps, Re = 11.8 x 10^5, nd/U = 5.96 x 10^{-2}.

The abscissa in these plots is ωt, where $\theta = \theta_o \sin \omega t$, and $0 < \omega t < 2\pi$ during one complete cycle. One interesting feature of these records is the irregularity of the aerodynamic torque which occurs when the disk is swinging back from $\theta = \pm \theta_o$ to $\theta = 0$. This is especially noticeable in Fig. 22 where the amplitude is large, $\theta_o = 0.707$ rad. This irregularity disappeared for the case of the sharp-edged disk in Fig. 25 where the torque appears to be close to the ideal sine wave. The evidence favors a hypothesis that the irregularity is associated with unsteady separation occurring on the edges of the thick disk, especially at larger amplitudes of oscillation. It can be seen that areas under all the work rate coefficient curves are negative, indicating that energy is transferred to the fluid medium. This result held true in all the forced oscillation tests. As a check, the data from Figs. 22 through 25 were used to plot M vs. θ and $M\dot{\theta}$ vs. t. The areas under these curves represent energy transfer per cycle and were found to give fair agreement (within about ± 20%) with the average energy rate data of the next section. Since Fig. 25 showed a very regular torque curve, the energy rate was calculated from the phase shift of the aerodynamic torque. If we define

$$\begin{aligned} \theta &= \theta_o \sin \omega t \\ M &= M_o \sin (\omega t + \phi) \end{aligned} \tag{11}$$

then it can be shown that the average work rate done by the fluid on the disk is

$$\bar{\dot{W}} = \frac{\omega M_o \theta_o}{2} \sin \phi \tag{12}$$

In Fig. 25 the phase lag is about 159°. This gives $\sin \phi = -0.358$ which means energy is put into the fluid and fair agreement was again obtained with the data of Section IV-2.

It is interesting in this connection, to examine Figs. 26 and 27 where we have data for pressure vs. motion and pressure phase lead on the front face of a freely oscillating disk. These data were taken with a piezoelectric pressure crystal mounted in a ported chamber in the disk. By sealing all the ports except one, the pressure variations at one location could be examined. According to our sign convention, pressures on the front face correspond to torques 180° out of phase with the pressures. Thus in interpreting Fig. 27 in terms of work rate, the sine of the phase angle shown is correct but it should now be considered a lag. Thus the pressures on the front face are tending to extract energy from the motion. We have no information about the pressure variations on the rear face of the disk where the flow is highly turbulent.

2. Average Rate of Energy Input to the Fluid. It is of interest to study the average rate of energy flow to the fluid as a function of the other test variables. This approach has the advantage that no assumptions are necessary regarding the type

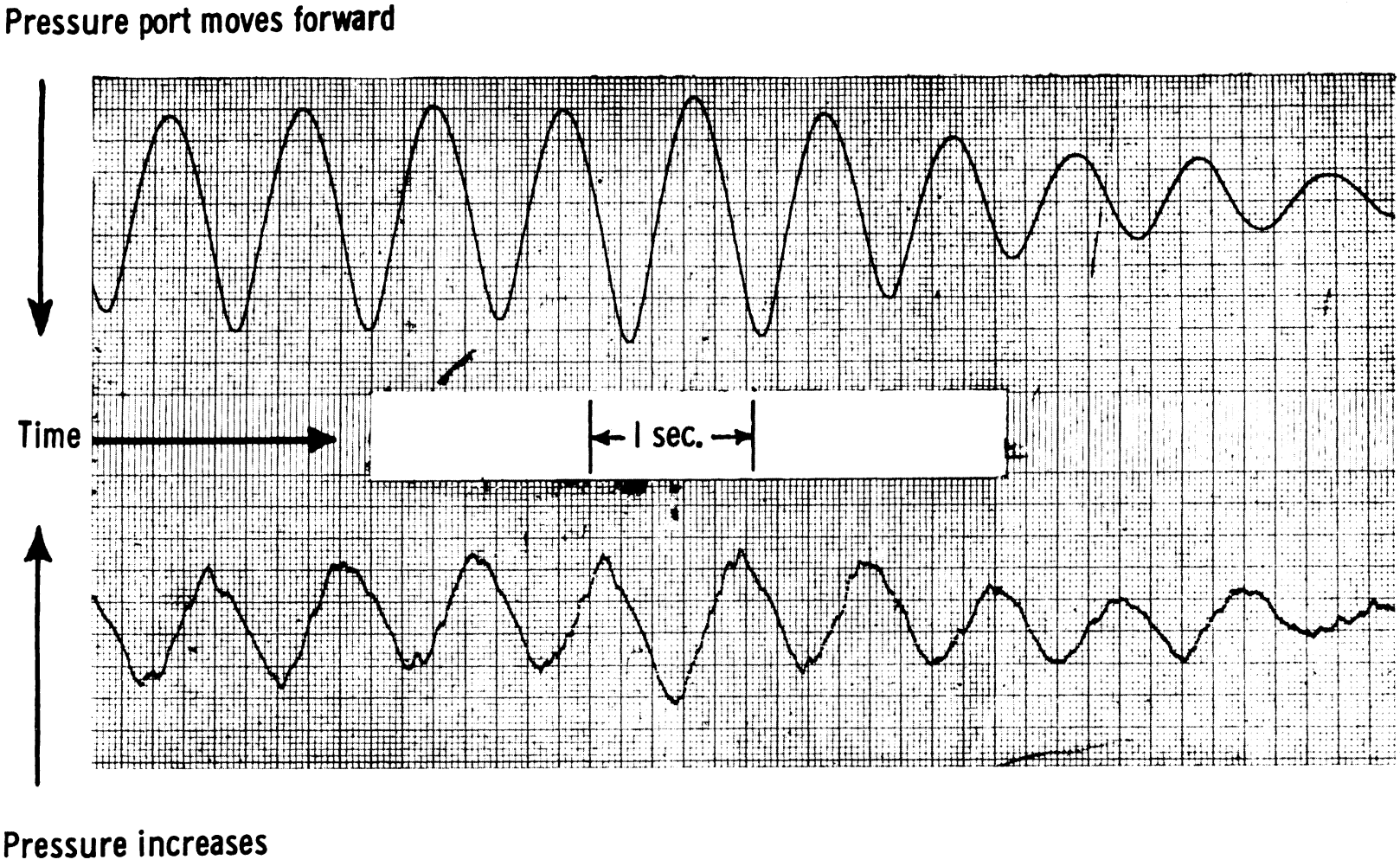

Fig. 26. Disk position angle, θ, and pressure on the face of the disk vs. time. d = 11 in., h/d = 0.034, I* = 2.17, nd/U = 0.0233. Pressure measured at 0.87 R along a diameter normal to the axis of rotation.

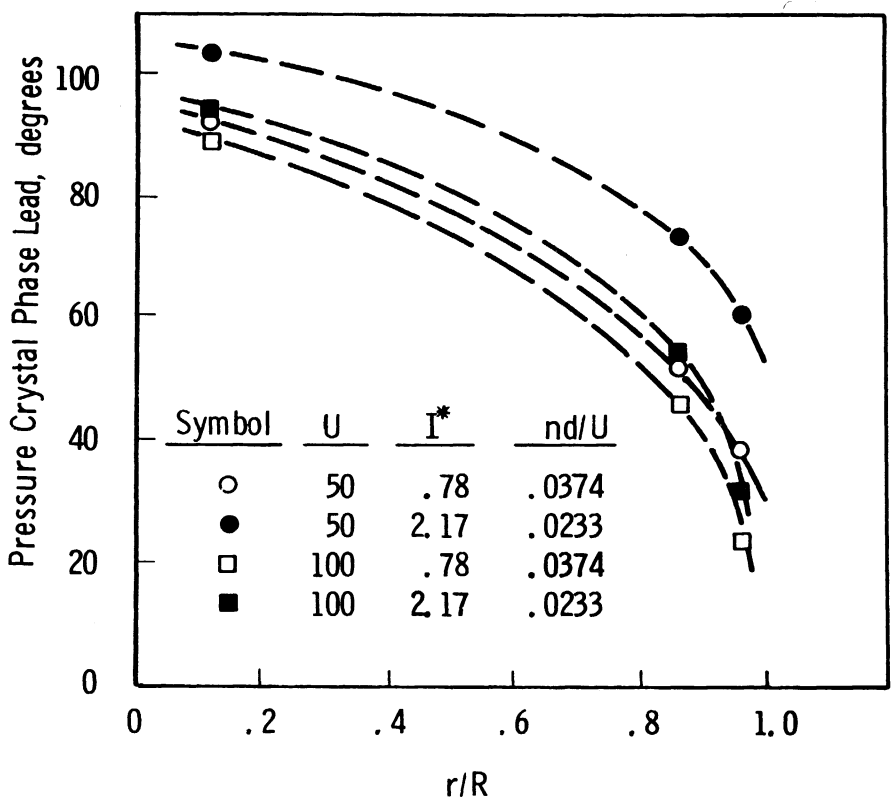

Fig. 27. Pressure phase lead as a function of position of the upstream face of a 0.92 ft diam disk in free oscillation. Pressure ports are located on a diameter normal to the oscillation axis.

of system (as is the case in measuring $C_{m\dot{\theta}}$). We assume that $\bar{\dot{W}}$ depends on ρ, μ, U, θ_o, and d. Then by dimensional analysis,

$$\frac{\bar{\dot{W}}}{qUS} = f\left\{\frac{nd}{U}, \theta_o, \frac{\rho Ud}{\mu}\right\} \tag{13}$$

It developed that Reynolds number did not have a strong effect, and that a moderately good unification of the data for three different amplitudes was possible by plotting $\bar{\dot{W}}/qUS$ against $nd\theta_o/U$ as in Fig. 28. The computer was calibrated for work rate by applying a known moment to the disk and electronically simulating a known $\dot{\theta}$ in the computer. The output of the multiplier in volts then corresponds to the known work rate in ft-lb/sec and the calibration constant is therefore established.

Physically, $nd\theta_o/U$ is proportional to the ratio of maximum disk edge velocity to

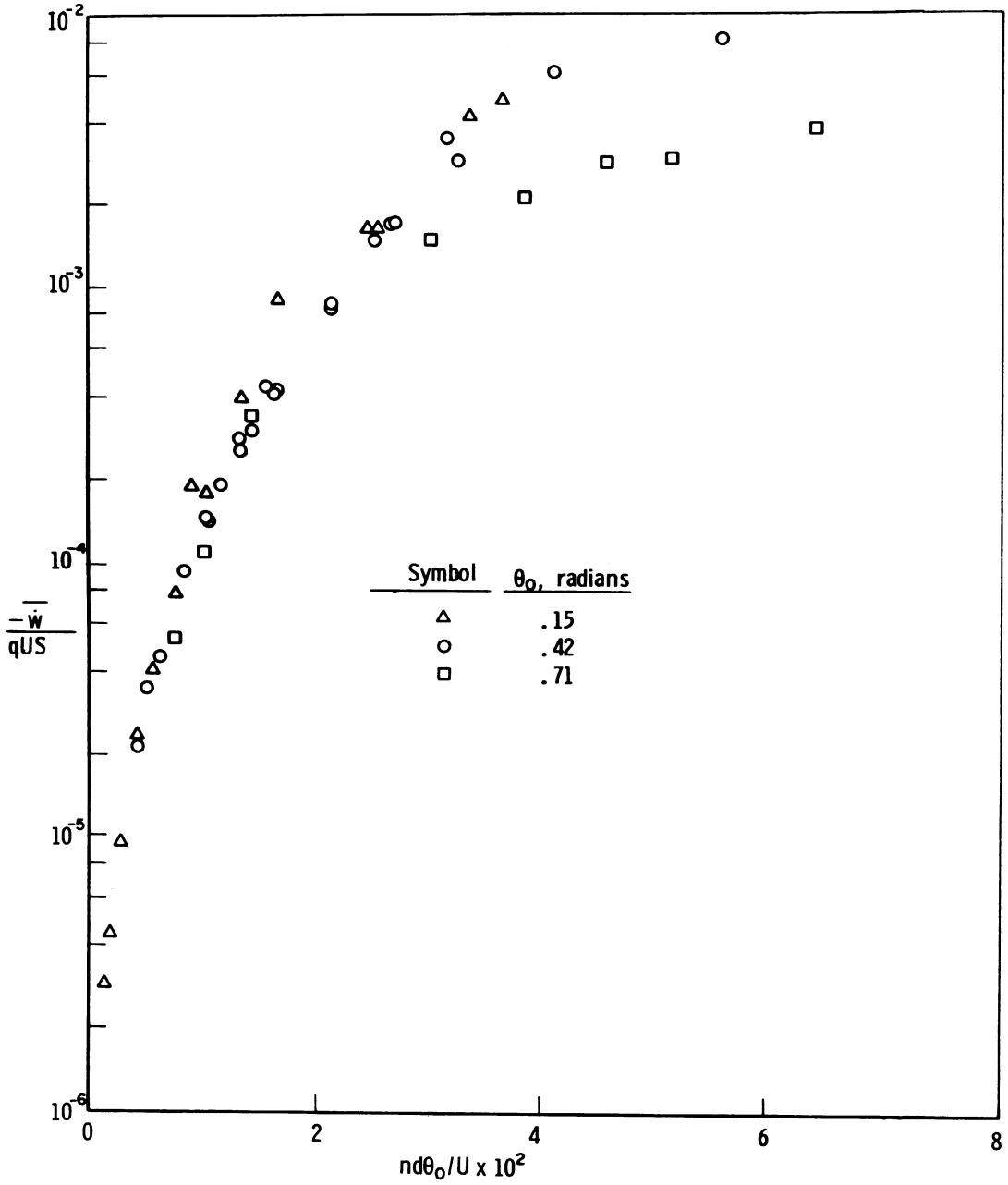

Fig. 28. Dimensionless average work rate as a function of $nd\theta_o/U$ for three amplitudes.

free stream velocity. Since the drag coefficient of a disk is near unity,* qUS can be thought of as the rate of energy addition to the fluid by disk drag if we take the point of view of an observer at rest with respect to the fluid. Thus $\bar{W}/qUS$ is approximately the ratio of energy put into the fluid by disk oscillation to the energy added by disk drag. From Fig. 28 it is seen that the maximum oscillation energy transfer to the fluid was of the order of 1% of the drag energy input to the fluid.

3. Damping Coefficient. The average work rate is,

$$\bar{\dot{W}} = \frac{1}{T}\int_0^T M\dot{\theta}dt \tag{14}$$

We assume sinusoidal motion of a second order linear system, where energy dissipation is caused by the linear viscous term. Then

$$\bar{\dot{W}} = \frac{\partial M}{\partial \dot{\theta}} \frac{1}{T}\int_0^T \dot{\theta}^2 dt \tag{15}$$

and since

$$\dot{\theta} = \theta_o \omega \cos \omega t$$

one can integrate to get for large T,

$$\bar{\dot{W}} = \frac{\partial M}{\partial \dot{\theta}} \left(\frac{\theta_o^2 \omega^2}{2}\right) = C_{m\dot{\theta}} \frac{qSd^2}{2U} \left(\frac{\theta_o^2 \omega^2}{2}\right) \tag{16}$$

Hence

$$C_{m\dot{\theta}} = \frac{4U}{qSd^2(\theta_o \omega)^2} \bar{\dot{W}} \tag{17}$$

which can be used to calculate the damping coefficient. In Fig. 29 we give the $C_{m\dot{\theta}}$ for three amplitudes as a function of nd/U. The shaded rectangle represents the measurements of the free oscillation damping coefficients. The damping coefficients measured in free oscillation are somewhat smaller than the damping coefficients found

*For $10^3 \leq Re \leq 10^6$ the drag coefficient of a thin circular disk is essentially constant at 1.17 (see Ref. 7).

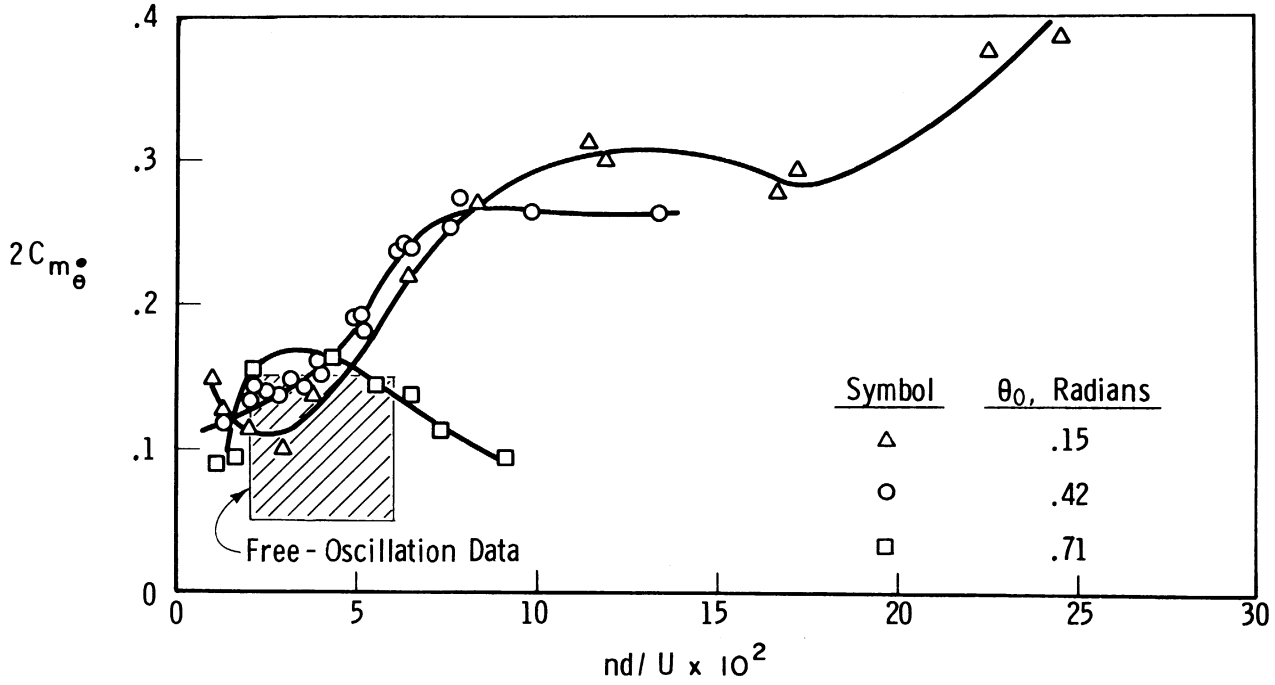

Fig. 29. Forced oscillation damping coefficient vs. nd/U for three amplitudes.

for forced oscillations. We do not have any explanation for this behavior. Another interesting feature is that the character of the damping curve for the largest amplitude, $\theta_0 = 0.71$, is somewhat different from the others, since it tends to drop as nd/U increases. It is possible that in swinging through large amplitudes, a disk edge intercepts vortices which have been previously shed from the opposite edge thereby altering the total energy addition to the fluid medium. At the lower amplitudes this interference would not occur, therefore an increase in the value of nd/U will increase the energy shed in vortices until interference between vortices shed by the edges occurs.

Another important feature of Fig. 29 is that $C_{m_{\dot{\theta}}}$ as a function of amplitude is nowhere a constant except in the region $4 < nd/U \times 10^2 < 5$ and $1 < nd/U \times 10^2 < 2$. In the region $2 < nd/U < 4$, $C_{m_{\dot{\theta}}}$ increases monotonically with amplitude. For the largest nd/U, $C_{m_{\dot{\theta}}}$ appears to decrease monotonically with amplitude (probably as a result of interference between shed vortices) and shows the largest of the measured values of $C_{m_{\dot{\theta}}}$ on the low amplitude curve ($\theta_0 = 0.15$).

Finally, we note that a 2.16 ft diam cardboard disk built around the 1.83 ft diam Styrofoam disk had essentially the same damping coefficient whether the edge was thick (2-1/2 in.) or thin (1/16 in.) for the case $\theta_0 = 0.42$ rad. The damping coefficients for these larger disks were in excellent agreement with the $\theta_0 = 0.42$ curve of Fig. 29. We recall that in Section V-1 the thin edge made the average moment much more regular, but it apparently did not affect the average energy dissi-

pation.

4. The Exciting Moment Produced by Turbulence. As already discussed, Section IV-A-4, the exciting moment is produced by turbulence in the disk wake. We have measured the mean square fluctuating moment acting on the 22 in. Styrofoam disk with the analog computer multiplier and we measured the power spectrum of the turbulent moment with the low frequency variable band pass filter whose readings were approximately corrected for band width variation.

The root mean square torque coefficient,

$$\sqrt{\overline{C_m'^2}} = \frac{\sqrt{\overline{M'^2}}}{qSd} \tag{18}$$

for various speeds is shown in Fig. 30 and is nearly a constant, in the available

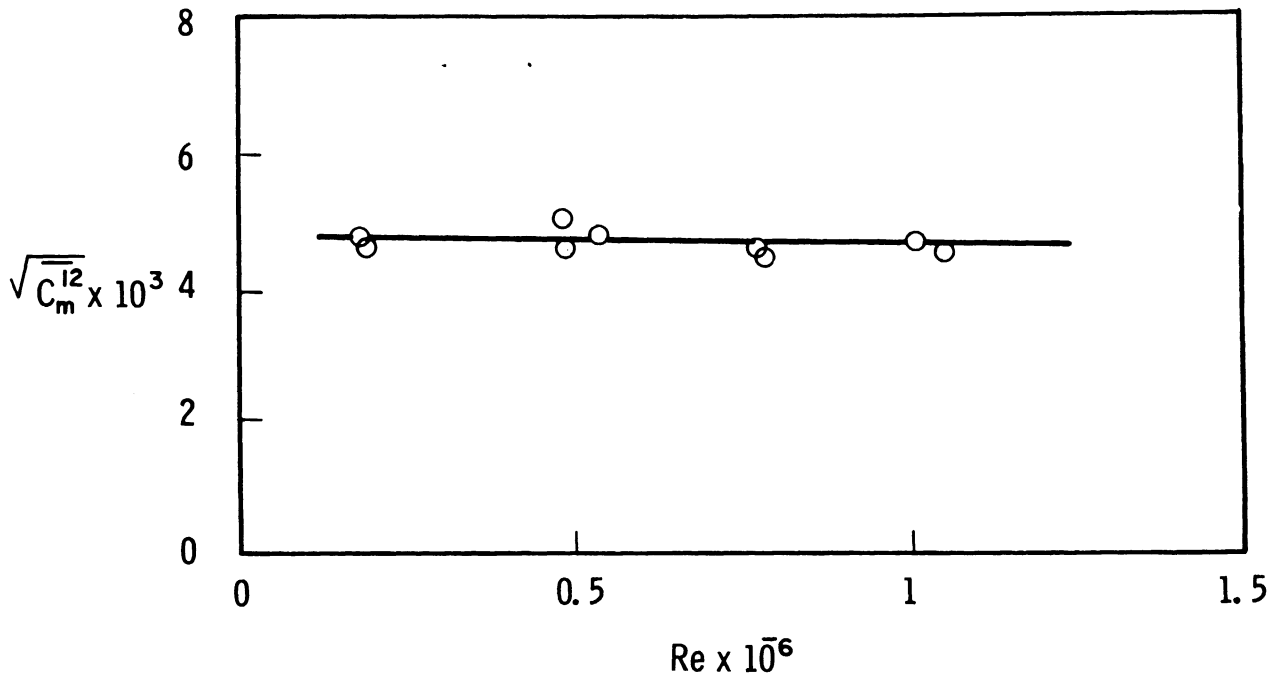

Fig. 30. Root mean square moment coefficient for the Styrofoam disk normal to flow ($\theta = 0$); d = 22 in., h = 2-3/8 in.

range of Reynolds number. We were restricted to the range $1 \times 10^5 < Re < 10 \times 10^5$ because at low speeds the moment signals were affected by tunnel wall vibration and electrical noise and at high speeds the disk drag can be large enough to damage the flexure pivots in the balance.

The power spectra of the turbulent torque, M(t), defined by

$$f_m(\omega) = \frac{2}{\pi}\int_0^\infty \overline{M'(t)M'(t+\tau)}\cos \omega\tau d\tau \tag{19}$$

were also measured and the results are shown in Fig. 31. The power spectra scaled with the wind tunnel speed, U. Because the power spectrum of the envelope amplitude for different diameter disks scaled with the characteristic time, d/U (see Section IV-A-4), we may conclude that the power spectrum of the exciting moment, M(t), would also scale with d/U. We have used this characteristic time in our Fig. 31 where the results of four tests at different speeds are shown.

Additional evidence that the turbulent wake produces the exciting moments causing the disk motion was obtained with the aerodynamic configuration shown in Fig. 7. A plywood disk with the same diameter, 22 in., as the Styrofoam disk was mounted 0.89 diam downstream of the Styrofoam disk. The root mean square fluctuating moment coefficient measured on the balance inside the Styrofoam disk was at first found to be very large (about twice the value without the plywood disk), when the tunnel was started and then fell to very small values of approximately $\sqrt{\overline{C_m'^2}} = 1.3 \times 10^{-3}$. The decrease was abrupt and was observed anywhere from 3 to 15 min after starting the tunnel. The next day the same test was run again and the fluctuating moment did not decrease even after running for a few hours. The value of root mean square fluctuating moment coefficient was $\sqrt{\overline{C_m'^2}} = 8.6 \times 10^{-3}$. These tests show that this configuration is very sensitive to the free stream turbulence which acts to "trigger" large turbulent fluctuations in the wake between the two disks. Brief observations of the motion of tufts placed between the two disks showed that severe turbulent fluctuations appeared whenever the fluctuating moment was large.

5. The Computation of the Root Mean Square Deflection Angle. Implicit in the formulation of the problem of disk oscillations as the random response of a linear system to a random input is the fact that the root mean square response can be computed if the power spectrum of the input and the properties of the system are known. The theory is discussed from a mathematical point of view in Ref. 6 and in a simple fashion with application to aerodynamic problems in Ref. 3. The result of the theory for the mean square amplitude of the response is that if the differential equation for the system is

$$\frac{d^2y}{dt^2} + \beta\frac{dy}{dt} + \omega_o^2 y = F(t) \tag{20}$$

where F(t) is the random input, the mean square of the random response is (see Ref. 3),

$$\overline{y^2} = \int_0^\infty \frac{f(\omega)d\omega}{(\omega^2-\omega_o^2)^2+\beta^2\omega^2} \tag{21}$$

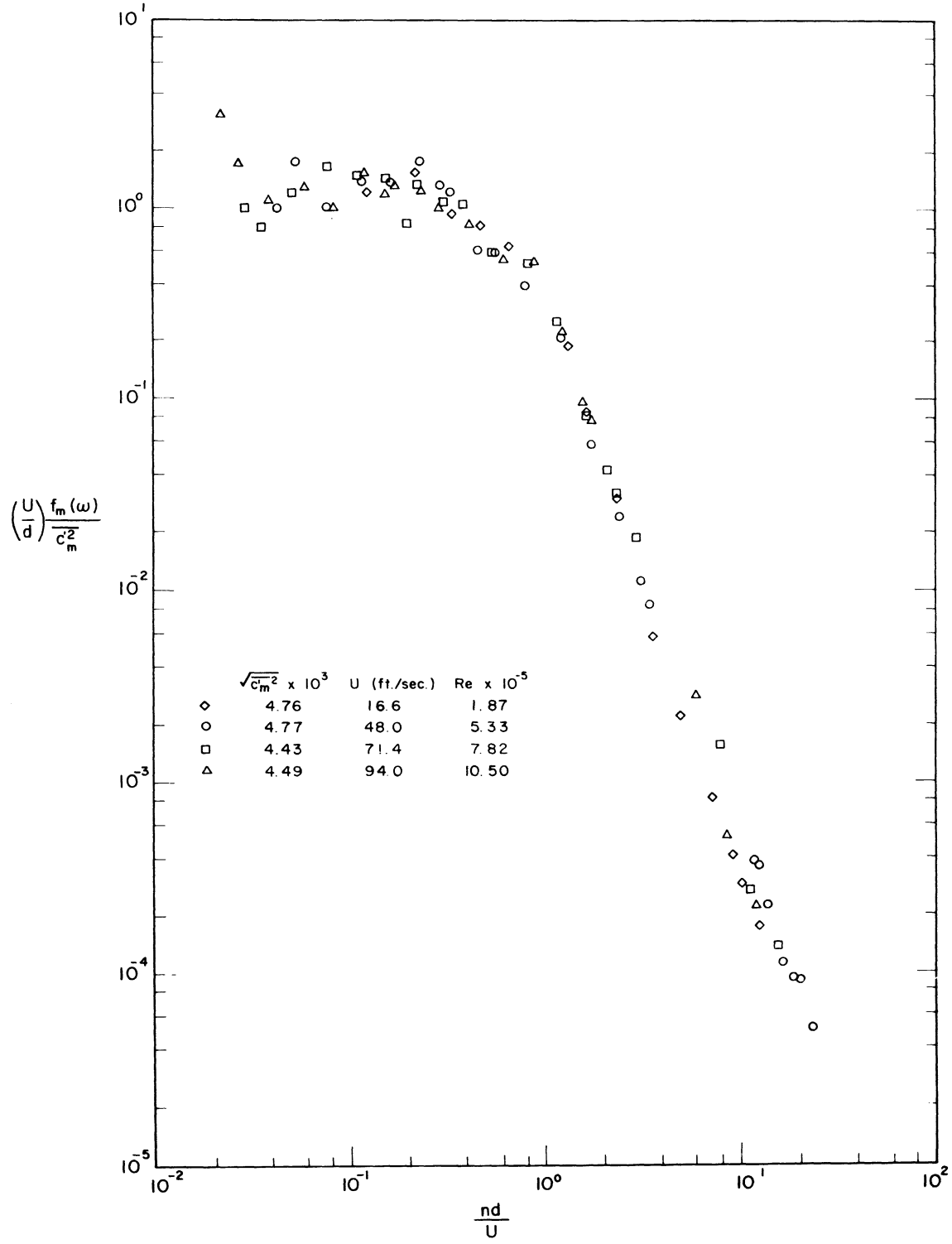

Fig. 31. Power spectra of the fluctuating aerodynamic moment acting on the Styrofoam disk normal to flow (θ = 0); d = 22 in., h = 2-3/8 in.

where $f(\omega)$ is the power spectrum of $F(t)$

$$f(\omega) = \frac{2}{\pi}\int_0^\infty \overline{F(t)F(t+\tau)}\cos\omega\tau d\tau \tag{22}$$

If $f(\omega)$ is a slowly varying function compared to the denominator of Eq. (21) (small damping β) one can write Eq. (22) in the approximate form

$$\overline{y^2} = f(\omega_o)\int_0^\infty \frac{d\omega}{(\omega^2-\omega_o^2)^2+\beta^2\omega^2} = \frac{\pi}{2}\frac{f(\omega_o)}{\beta\omega_o^2} \tag{23}$$

We refer to our Eq. (1) and making the appropriate substitutions from it in Eq. (21) we find that the mean square angular position of the disk is

$$\overline{\theta^2} = \frac{\pi}{2}\left(\frac{U}{d}\right)\left[\frac{f_m(\omega_o)}{\overline{C_m'^2}}\right]\frac{\overline{C_m'^2}}{C_{m_{\dot\theta}}C_{m_\theta}} \tag{24}$$

where the spectral density of the turbulent moment, $f_m(\omega_o)$, is evaluated at the natural frequency of disk oscillations.

We have chosen the case of an aluminum disk mounted on a knife edge for our computation of $\overline{\theta^2}$. For this disk the values of the parameters appearing in Eq. (24) are from Table I,

$\omega_o d/U = .192$

$\frac{U}{d}\frac{f_m(\omega_o)}{\overline{C_m'^2}} = 1.4$

$\sqrt{\overline{C_m'^2}} = 4.7 \times 10^{-3}$

$C_{m_\theta} = .161$

$C_{m_{\dot\theta}} = .05$

Inserting these values in Eq. (24) the result is

$$\sqrt{\overline{\theta^2}} = .078 \tag{25}$$

The measured value for this case was $\sqrt{\overline{\theta^2}} = 0.122$. Thus the measured value of $\sqrt{\overline{\theta^2}}$ is 1.5 times as large as the calculated value. We do not know the reason for the difference between the values. We suggest that the static restoring moment coefficient,

TABLE I

Run	I*	U(fps)	d(ft)	n/d x 10^2	$\omega d/U$	Pivot	Re x 10^{-5}	$\sqrt{\overline{\theta^2}}$ x 10
1	1.306	53.7	0.5	1.04	.189	BB	1.68	0.996
2	1.306	101.4	0.5	1.04	.176	BB	3.25	0.88
3	1.125	52.4	1.0	1.04	.194	KE	3.35	1.28
4	1.125	52.6	1.0	1.04	.192	KE	3.35	1.26
5	1.125	52.9	1.0	1.04	.201	KE	3.28	1.211
6	1.125	53.3	1.0	1.04	.195	KE	3.31	1.21
7	1.125	102.3	1.0	1.04	.192	KE	6.16	1.218
8	1.125	52.0	1.0	1.04	.194	BB	3.13	0.806
9	1.125	35.6	1.0	1.04	.191	BB	2.15	0.826
10	1.125	99.9	1.0	1.04	.188	BB	6.02	0.815
11	14.1	102.0	0.5	4.16	.025	BB	6.14	0.161
12	14.1	54.0	0.5	4.16	.061	BB	3.25	0.236
13	14.1	79.1	0.5	4.16	.060	BB	4.77	0.347
14	14.1	102.0	0.5	4.16	.060	BB	6.14	0.314
15	42.3	27.5	0.5	12.48	none	BB	1.61	0.087
16	42.3	55.0	0.5	12.48	.040	BB	3.22	0.253
17	42.3	78.4	0.5	12.48	.034	BB	4.58	0.264
18	42.3	102.5	0.5	12.48	.034	BB	6.00	0.410

$C_{m\theta}$, we have used may be larger than the actual restoring moment and we recall that the damping moment coefficient from the free oscillation tests was lower than the forced oscillation coefficient that we have used.

We can conclude that the representation of Eq. (1) for the oscillating disk is only approximate and gives a good qualitative and an approximate quantitative description of the phenomena. A large factor in the lack of good quantitative agreement is probably the variation of $C_{m\theta}$ with θ and the dependence of $C_{m\dot{\theta}}$ on nd/U.

V. CONCLUSIONS

Studies of the free oscillations of thin disks constrained to rotate about a diameter through their center reveal that the observed random disk oscillations can be qualitatively explained within the framework of the linear aerodynamic force representation and the theory for forced random oscillations of a linear system. In the present case the impressed forcing function is found to originate in the turbulent fluctuations in the disk wake.

As was mentioned before, the linear theory assumes constant aerodynamic derivatives for the representation of the aerodynamic restoring moment and damping moment. Furthermore these moments are assumed to be independent of the impressed turbulent exciting moment. It appears that important deviations from the linear theory have prevented quantitative agreement of the root mean square deflection of the disk computed from the linear theory with the measured root mean square deflection. The experimentally measured value of $\sqrt{\overline{\theta^2}}$ was 1.5 times as large as the computed value of $\sqrt{\overline{\theta^2}}$.

The measured statistical properties of the disk motion show that turbulence generated behind a grid causes a change in the probability distribution of the disk amplitude but no change in $\sqrt{\overline{\theta^2}}$. The measurements of the fluctuating exciting moment acting on the disk when a second disk was mounted behind the first showed that the moment fluctuations would be greatly suppressed or greatly increased when the turbulence level in the tunnel changed during the tunnel starting process.

APPENDIX A

Consider a rigid body free to rotate about a fixed axis. If the angular position of the body is denoted by θ the equation of motion of the body is

$$I \frac{d^2\theta}{dt^2} = M(t) \tag{A-1}$$

where t is the time. The torque acting on the body, M(t), is defined positive in the same direction as the sense of rotation and I is the moment of inertia of the body. The torque acting on the disk that is produced by the aerodynamic forces is a function of the body geometry, motion, and properties of the fluid. For the present purpose we write the approximate linearized expression,

$$M(t) = - \frac{\partial M}{\partial \theta} \theta(t) - \frac{\partial M}{\partial \dot{\theta}} \frac{d\theta}{dt} + M'(t) \tag{A-2}$$

where $\dot{\theta}$ is the time derivative of θ. Implicit in this equation is the assumption that the motion of the body introduces only small disturbances of the torque and M(t). It is also assumed that the unsteady component of the torque produced by turbulence does not depend on the body motion.

The expression (A-2) can now be introduced into Eq. (A-1).

$$I \frac{d^2\theta}{dt^2} + \frac{\partial M}{\partial \dot{\theta}} \frac{d\theta}{dt} + \frac{\partial M}{\partial \theta} \theta = M'(t) \tag{A-3}$$

By introducing a dimensionless time, $tU/d = t'$, where U is the stream velocity, and dividing (4) by $\rho(U^2/2)(\pi d^3/4)$ where ρ is the fluid density we obtain

$$I_1^* \frac{d^2\theta}{dt'^2} + C_{m\dot{\theta}} \frac{d\theta}{dt'} + C_{m\theta}\theta = C_m'(t') \tag{A-4}$$

Here,

$$
\begin{aligned}
I_1^* &= \frac{8}{\pi} I^* \\
C_{m_{\dot\theta}} &= \frac{\partial M / \partial \left(\frac{\dot\theta d}{U}\right)}{qSd} \\
C_{m_\theta} &= \frac{\partial M / \partial \theta}{qSd} \\
C_m' &= \frac{M'}{qSd}
\end{aligned}
\tag{A-5}
$$

We note that in conventional aerodynamic terminology (see Ref. 8 for example),

$$2C_{m_{\dot\theta}} = -(C_{m_q} + C_{m_{\dot\alpha}}) \tag{A-6}$$

$$C_{m_\theta} = -C_{m_\alpha} \tag{A-7}$$

where the aerodynamic coefficients including C_m' are functions of Reynolds number, Mach number, and h/d.

The properties of (A-4) describing a second order linear system with input $C_m'(t')$ and output $\theta(t')$ can now be discussed in terms of the aerodynamic and mechanical parameters governing the motion. We can obtain an expression for the natural frequency of oscillation of the system by assuming periodic solutions of the form $e^{\lambda t}$ and inserting this into Eq. (A-4) with $C_m'(t) = 0$. The roots of the resulting algebraic equation are

$$\lambda_1, \lambda_2 = -\frac{C_{m_{\dot\theta}}}{2I_1^*} \pm \sqrt{\left(\frac{C_{m_{\dot\theta}}}{2I_1^*}\right)^2 - \frac{C_{m_\theta}}{I_1^*}} \tag{A-8}$$

so that for $C_{m_{\dot\theta}}^2 < 4C_{m_\theta} I_1^*$, oscillatory solutions with frequency

$$\frac{\omega d}{U} = \frac{2\pi n d}{U} = \sqrt{\frac{C_{m_\theta}}{I_1^*} - \left(\frac{C_{m_{\dot\theta}}}{2I_1^*}\right)^2} \tag{A-9}$$

are possible. The dimensionless frequency of natural oscillations varies as $(I^*)^{-.50}$ if C_{m_θ} is constant and $C_{m_{\dot\theta}} = 0$.

The damping coefficient $C_{m\dot{\theta}}$ can be obtained from records of damped sinusoidal motion as follows: From the roots λ_1, λ_2, Eq. (A-8), the amplitude damping law is,

$$\theta_o(t') = \theta_o(o)e^{-C_{m\dot{\theta}}t'/2I_1^*}; \qquad t' = \frac{tU}{d} \tag{A-10}$$

Therefore,

$$\ln \frac{\theta_o(t')}{\theta_o(o)} = -\frac{C_{m\dot{\theta}}t'}{2I^*} = -\frac{C_{m\dot{\theta}}}{I^*}\frac{\pi}{16}\frac{Ut}{d} \tag{A-11}$$

Now consider

$$\frac{\omega t}{2\pi} = N$$

where N is the number of cycles elapsed since t = 0. Thus we substitute

$$t = \frac{2\pi N}{\omega} \tag{A-12}$$

to obtain

$$\ln \frac{\theta_o(t')}{\theta_o(o)} = -C_{m\dot{\theta}}\frac{\pi^2}{8}\frac{N}{I^*\omega^*} \tag{A-13}$$

or using the base 10 for the logarithm,

$$\log \frac{\theta_o(t')}{\theta_o(o)} = -C_{m\dot{\theta}}(\log e)\left(\frac{\pi^2}{8}\right)\left(\frac{N}{I^*\omega^*}\right) \tag{A-14}$$

REFERENCES

1. Willmarth, W. W., Hawk, N. E., and Harvey, R. L., "Investigations of the Steady and Unsteady Motion of Freely Falling Disks," ARL Report 63-176, October, 1963.

2. Lin, C. C., "On the Motion of a Pendulum in a Turbulent Fluid," Quart. Appl. Math., 1, No. 1, April, 1943.

3. Liepmann, H. W., "On the Application of Statistical Concepts to the Buffeting Problem," J. Aeron. Sci., 19, No. 12, December, 1952.

4. Liepmann, H. W., "Aspects of the Turbulence Problem," J. Appl. Math. and Phys. (ZAMP), III, 1952.

5. Fung, Y. C., An Introduction to the Theory of Aeroelasticity, Galcit Aeronautical Series, John Wiley and Sons, Inc., 1955.

6. Davenport and Root, An Introduction to the Theory of Random Signals and Noise, McGraw-Hill Book Co., Inc., 1958, p. 145.

7. Hoerner, S. F., Fluid Dynamic Drag, published by Sighard F. Hoerner, 1958.

8. Etkin, B., Dynamics of Flight, John Wiley and Sons, Inc., 1959.